Article

Cell Reports

Targeting Excessive EZH1 and EZH2 Activities for Abnormal Histone Methylation and Transcription Network in Malignant Lymphomas

Graphical Abstract

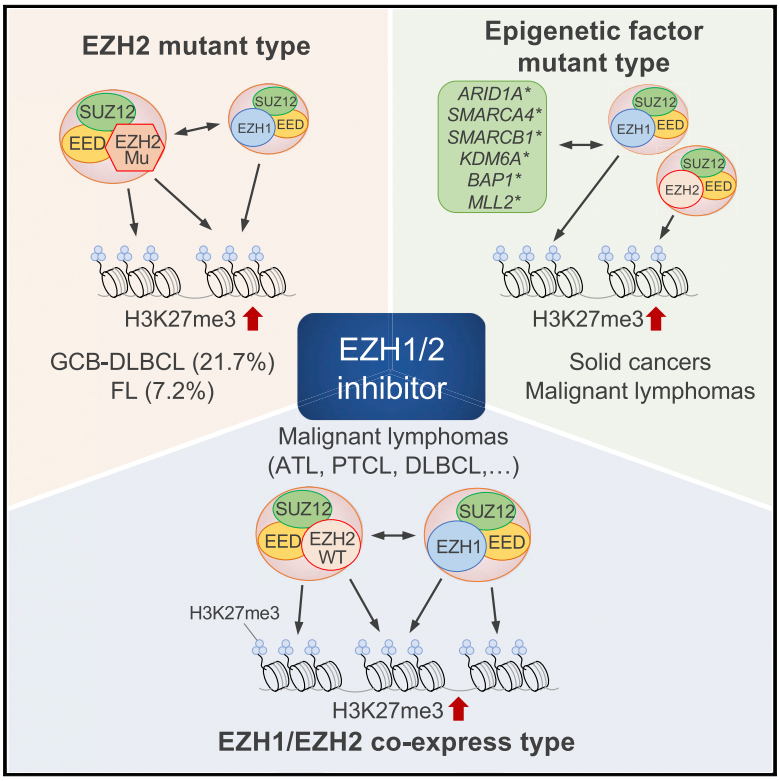

Highlights

- Lymphoma transcriptome is under control of global H3K27me3 accumulation
- EZH1 and EZH2 are druggable targets in *EZH2*$^{WT/WT}$ and *EZH2*$^{WT/Mu}$ malignancies
- Inactivation of chromatin-associated genes triggers EZH1/2 perturbation
- Targeting epigenome for pre-cancerous states is achieved by EZH1/2 inhibition

Authors

Makoto Yamagishi, Makoto Hori, Dai Fujikawa, ..., Kazushi Araki, Toshiki Watanabe, Kaoru Uchimaru

Correspondence

myamagishi@edu.k.u-tokyo.ac.jp (M.Y.), uchimaru@cbms.k.u-tokyo.ac.jp (K.U.)

In Brief

A mechanism-based, effective strategy for controlling oncogenic H3K27me3 remains an open question. Yamagishi et al. provide the scientific rationale for dual targeting of EZH1+EZH2 in malignancies overexpressing EZH2, such as ATL, PTCL, and DLBCL, or harboring mutations in histone-modifying genes, as well as in pre-cancerous cells epigenomically perturbed by oncovirus infection.

Yamagishi et al., 2019, Cell Reports *29*, 2321–2337
November 19, 2019
https://doi.org/10.1016/j.celrep.2019.10.083

CellPress

Cell Reports
Article

Targeting Excessive EZH1 and EZH2 Activities for Abnormal Histone Methylation and Transcription Network in Malignant Lymphomas

Makoto Yamagishi,[1,17,*] Makoto Hori,[1] Dai Fujikawa,[2] Takeo Ohsugi,[3] Daisuke Honma,[4] Nobuaki Adachi,[5] Harutaka Katano,[6] Tsunekazu Hishima,[7] Seiichiro Kobayashi,[8] Kazumi Nakano,[1] Makoto Nakashima,[1] Masako Iwanaga,[9] Atae Utsunomiya,[10] Yuetsu Tanaka,[11] Seiji Okada,[12] Kunihiro Tsukasaki,[13] Kensei Tobinai,[14] Kazushi Araki,[15] Toshiki Watanabe,[16] and Kaoru Uchimaru[1,*]

[1]Department of Computational Biology and Medical Sciences, Graduate School of Frontier Sciences, The University of Tokyo, Tokyo, Japan
[2]Animal Models and Retroviral Vaccines Section, Vaccine Branch, Center for Cancer Research, National Cancer Institute, NIH, Bethesda, MD, USA
[3]Department of Laboratory Animal Science, School of Veterinary Medicine, Rakuno Gakuen University, Hokkaido, Japan
[4]Oncology Laboratories, Daiichi Sankyo, Co., Tokyo, Japan
[5]Biomarker Department, Daiichi Sankyo, Co., Tokyo, Japan
[6]Department of Pathology, National Institute of Infectious Diseases, Tokyo, Japan
[7]Department of Pathology, Tokyo Metropolitan Cancer and Infectious Diseases Center Komagome Hospital, Tokyo, Japan
[8]Division of Molecular Therapy, Institute of Medical Science, The University of Tokyo, Tokyo, Japan
[9]Department of Clinical Epidemiology, Graduate School of Biomedical Sciences, Nagasaki University, Nagasaki, Japan
[10]Department of Hematology, Imamura General Hospital, Kagoshima, Japan
[11]Graduate School and Faculty of Medicine, University of the Ryukyus, Okinawa, Japan
[12]Joint Research Center for Human Retrovirus Infection, Graduate School of Medical Sciences, Kumamoto University, Kumamoto, Japan
[13]Department of Hematology, International Medical Center, Saitama Medical University, Saitama, Japan
[14]Department of Hematology, National Cancer Center Hospital, Tokyo, Japan
[15]Oncology Clinical Development Department, Daiichi Sankyo Co., Tokyo, Japan
[16]Future Center Initiative, The University of Tokyo, Tokyo, Japan
[17]Lead Contact
*Correspondence: myamagishi@edu.k.u-tokyo.ac.jp (M.Y.), uchimaru@cbms.k.u-tokyo.ac.jp (K.U.)
https://doi.org/10.1016/j.celrep.2019.10.083

SUMMARY

Although global H3K27me3 reprogramming is a hallmark of cancer, no effective therapeutic strategy for H3K27me3-high malignancies harboring *EZH2*$^{WT/WT}$ has yet been established. We explore epigenome and transcriptome in *EZH2*$^{WT/WT}$ and *EZH2*$^{WT/Mu}$ aggressive lymphomas and show that mutual interference and compensatory function of co-expressed EZH1 and EZH2 rearrange their own genome-wide distribution, thereby establishing restricted chromatin and gene expression signatures. Direct comparison of leading compounds introduces potency and a mechanism of action of the EZH1/2 dual inhibitor (valemetostat). The synthetic lethality is observed in all lymphoma models and primary adult T cell leukemia-lymphoma (ATL) cells. Opposing actions of EZH1/2-polycomb and SWI/SNF complexes are required for facultative heterochromatin formation. Inactivation of chromatin-associated genes (*ARID1A*, *SMARCA4/BRG1*, *SMARCB1/SNF5*, *KDM6A/UTX*, *BAP1*, *KMT2D/MLL2*) and oncovirus infection (HTLV-1, EBV) trigger EZH1/2 perturbation and H3K27me3 deposition. Our study provides the mechanism-based rationale for chemical dual targeting of EZH1/2 in cancer epigenome.

INTRODUCTION

Histone H3 regulation, particularly H3 lysine 27 trimethylation (H3K27me3), is a central process for chromatin condensation and gene silencing. The suppressive histone mark is catalyzed by polycomb repressive complex 2 (PRC2), which includes either enhancer of zeste homolog 1 (EZH1) or EZH2 as an enzymatically active core subunit, as well as other components, such as EED and SUZ12. A heterozygous gain-of-function (GoF) mutation of *EZH2* has been observed in certain lymphoma types, contributing to increased H3K27me3 (Morin et al., 2010; Béguelin et al., 2013). In contrast, many other cancer types, including the majority of malignant lymphomas and various solid tumors, also show overexpression of EZH2 and global H3K27me3 accumulation irrespective of *EZH2* gene mutation (Comet et al., 2016; Fujikawa et al., 2016). Epigenomic studies, particularly those addressing chromatin and transcription regulation, have demonstrated that inappropriate H3K27me3 deposition is a critical determinant of the abnormal transcriptome of various cancers (Pfister and Ashworth, 2017; Yamagishi and Uchimaru, 2017).

Because H3K27me3 is an enzymatic product, this reversible property provides a good foundation for the development of epigenetic drugs. Several small compounds have been

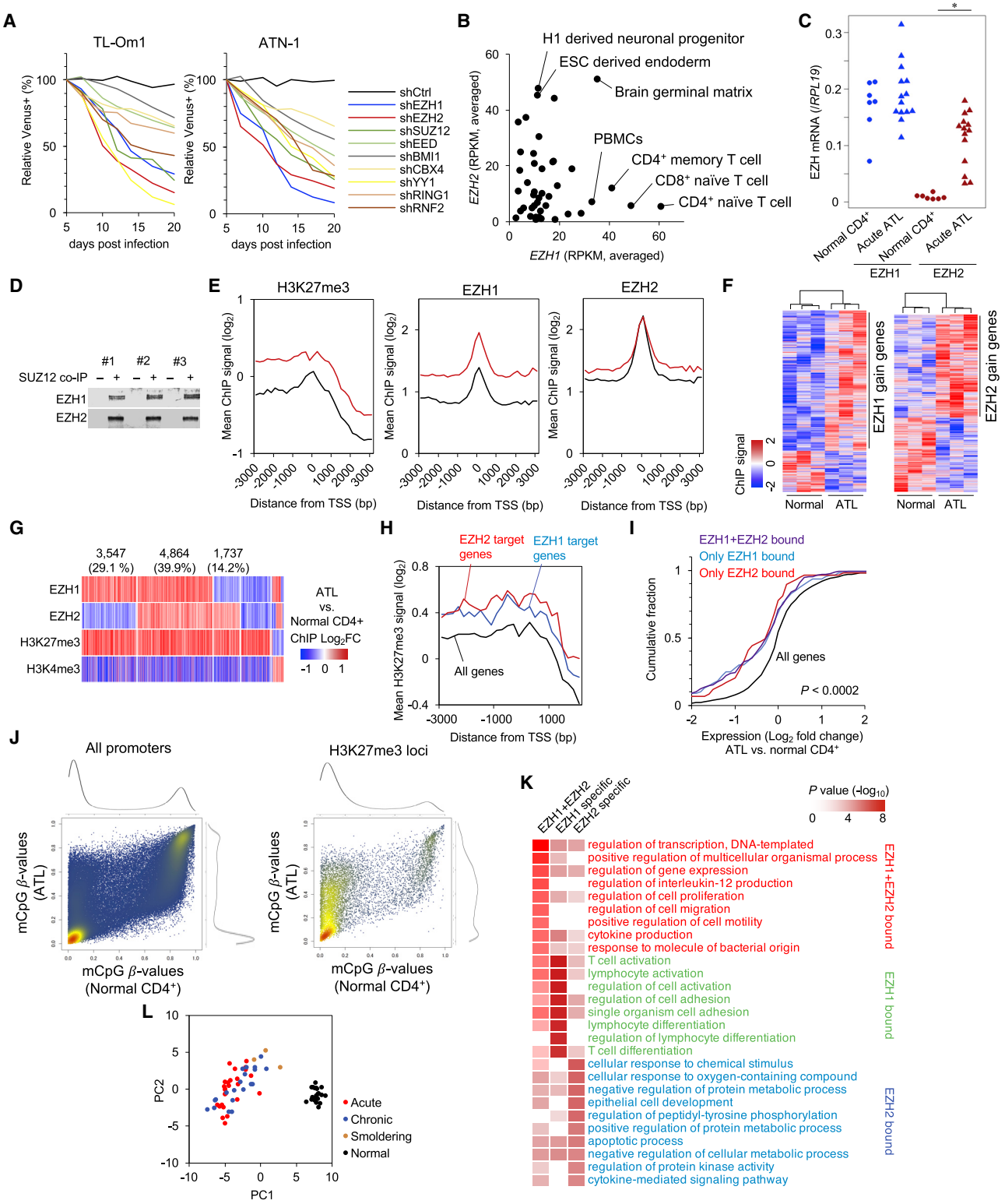

Figure 1. EZH1- and EZH2-Dependent H3K27me3 Accumulation

(A) ATL cell lines were transduced with shRNA lentivirus vectors. Venus-positive population transduced with shRNA series are plotted (representative data, n = 2 biological replicates).

(B) *EZH1* (x axis) and *EZH2* (y axis) levels in various normal cell types.

(legend continued on next page)

developed as potential EZH2 inhibitors (McCabe et al., 2012; Knutson et al., 2013; Qi et al., 2012; Bradley et al., 2014), as well as EZH1/2 dual inhibitors (Xu et al., 2015a; Honma et al., 2017). The inhibitors of the methyltransferase activity diminish the abundance of H3K27me3 and decrease the growth of cancer cells harboring *EZH2* GoF mutations. In addition, recent clinical study further reported the potential safety and efficacy of the EZH2 inhibitor against the *EZH2* mutant B cell lymphomas (Italiano et al., 2018). However, these studies concurrently suggest that H3K27me3-high malignancies harboring $EZH2^{WT/WT}$ are relatively tolerant to EZH2 inhibitors.

Only two enzymes catalyze H3K27me3 in mammalian cells. The importance of EZH1 in chromatin regulation has also been pointed out (Shen et al., 2008; Margueron et al., 2008). A cancer panel assay *in vitro* and some *in vivo* models suggested that the EZH1/2 dual inhibitors have efficacy against several cancer types (Honma et al., 2017). However, the underlying mechanisms of gene silencing and therapeutic efficacies of the epigenetic drugs remain under discussion, because of a lack of data representing the dynamic action of the corresponding histone methyltransferases and other chromatin regulators. The functional distribution and molecular dynamics of PRC2-EZH1 and PRC2-EZH2 on the abnormal H3K27me3 pattern remain unknown, which may prevent the clinical development and appropriate use of drugs targeting H3K27me3. In addition, molecular responses following exposure to an EZH2 inhibition remain to be elucidated. In order to precisely control "oncogenic H3K27me3" by the aforementioned leading compounds, drug evaluation by the unified index may also be required.

Here, we explored the regulatory mechanism of H3K27me3 in both $EZH2^{WT/WT}$ and $EZH2^{WT/Mu}$ malignancies. We show that the chromatin distributions of EZH1 and EZH2 are reciprocally reprogrammed and tightly involved in global histone methylation in aggressive lymphomas. Direct comparisons of the several inhibitors suggest that dual inhibition of EZH1 and EZH2 is required for strong synthetic lethality in malignancies overexpressing EZH2 or harboring mutations to histone-modifying genes, as well as in precancerous cells epigenetically perturbed by oncovirus infection.

RESULTS

Many cancers are characterized by abnormal upregulation of the H3K27me3 promoter. In adult T cell leukemia-lymphoma (ATL), H3K27me3-mediated gene repression (Fujikawa et al., 2016) was found to be correlated with poor prognostic markers (Iwanaga et al., 2010; Katsuya et al., 2012) (Figures S1A and S1B). Global gene downregulation, including that of important genes for leukemogenesis and also targets of genetic lesions (Kataoka et al., 2015), was associated with H3K27me3 accumulation (Figures S1C and S1D). H3K27me3 was acquired at originally unmethylated promoters in ATL cells, suggesting neomorphic functions of the polycomb family with $EZH2^{WT/WT}$ (Fujikawa et al., 2016) (Figure S1E).

EZH1- and EZH2-Dependent H3K27me3 Accumulation in ATL

We tested the functional importance of PRC1/2 components using short hairpin RNA (shRNA)-mediated gene knockdown (KD) screening in two ATL-derived cell lines. Selective reduction of proliferation was observed in the PRC-defective cells (Figures 1A and S2A). In particular, EZH1 and EZH2 were found to be independently required for ATL cell proliferation (Figure S2B). RNA sequencing (RNA-seq) data (Kundaje et al., 2015) showed that *EZH1* and *EZH2* genes were reciprocally regulated in physiological states (Figures 1B and S2C). Some cell types, such as from epithelial tissues, express low *EZH1* and *EZH2*, and undifferentiated H3K27me3-high embryonic stem and progenitors express low *EZH1* but high *EZH2*. Mature lymphocytes, such as $CD4^+$ T cells, express high *EZH1*, low *EZH2*, and stable PRC components. *KDM6B*, which encodes the H3K27me3 demethylase JMJD3, was highly expressed in almost all cell types, suggesting that basal H3K27 methylation is tightly regulated. qRT-PCR and transcriptome data (Yamagishi et al., 2012) revealed that *EZH1* was stably expressed and *EZH2* was significantly overexpressed with promoter H3K4me3 deposition in ATL cells (Figures 1C, S2D, and S2E). *KDM6B* was epigenetically silenced with high H3K27me3 in ATL cells. Co-immunoprecipitation assays (co-IP) of primary malignant cells showed that both EZH1 and EZH2 coexisted with SUZ12, suggesting that both enzymes are functionally active in PRC2 (Figure 1D). Although not selected as a candidate of molecular target when considering the expression changes between normal and malignant cells, functional screening suggested the importance of EZH1.

Because epigenetic control is a dynamic process, transition of the epigenetic landscape from a normal to a cancerous state could reveal the epigenetic alterations associated with disease

(C) *EZH1* and *EZH2* mRNA levels in normal $CD4^+$ T cells (n = 7) and acute-type ATL cells (n = 14). *$p < 10^{-5}$.
(D) Nuclear cell extracts from primary leukemic cells from acute ATL patients (n = 3) were immunoprecipitated with anti-SUZ12 antibody (+) or control IgG (−) and analyzed using immunoblotting.
(E) Mean ChIP values of H3K27me3, EZH1, and EZH2 of all genes in ATL cells (red) and normal $CD4^+$ T cell (black). n = 3.
(F) Differential chromatin occupancy of EZH1 and EZH2 (ChIP fold change [FC] > 2 [gain] and < −2 [loss] versus normal T cells, n = 3).
(G) Global views of the epigenetic changes (log FC mean values) at H3K27me3 altered genes (H3K27me3 ChIP abs[FC] > 1.5, 12,943 genes, 77.7% of data available, 16,654 genes).
(H) Mean H3K27me3 values of EZH1 and EZH2 targets and all genes in ATL (n = 3).
(I) Cumulative distributions of expression changes of EZH1/2 targets in acute-type ATL (n = 26) versus normal $CD4^+$ T cells (n = 21). $p < 0.0002$, Kolmogorov-Smirnov test.
(J) Genome-wide DNA CpG methylation pattern in normal $CD4^+$ versus ATL (n = 3). Averaged β values and density distributions of all promoter (left) and H3K27me3-accumulated sites (right) are plotted.
(K) GO analysis of EZH1- and EZH2-bound silenced genes (H3K27me3 ChIP FC > 1.5, EZH1 or EZH2 ChIP FC > 2, expression FC < −2).
(L) PCA clustering on the basis of expression of the EZH1/2 target genes in ATL (n = 49) and normal T cells (n = 21).
See also Figures S1 and S2.

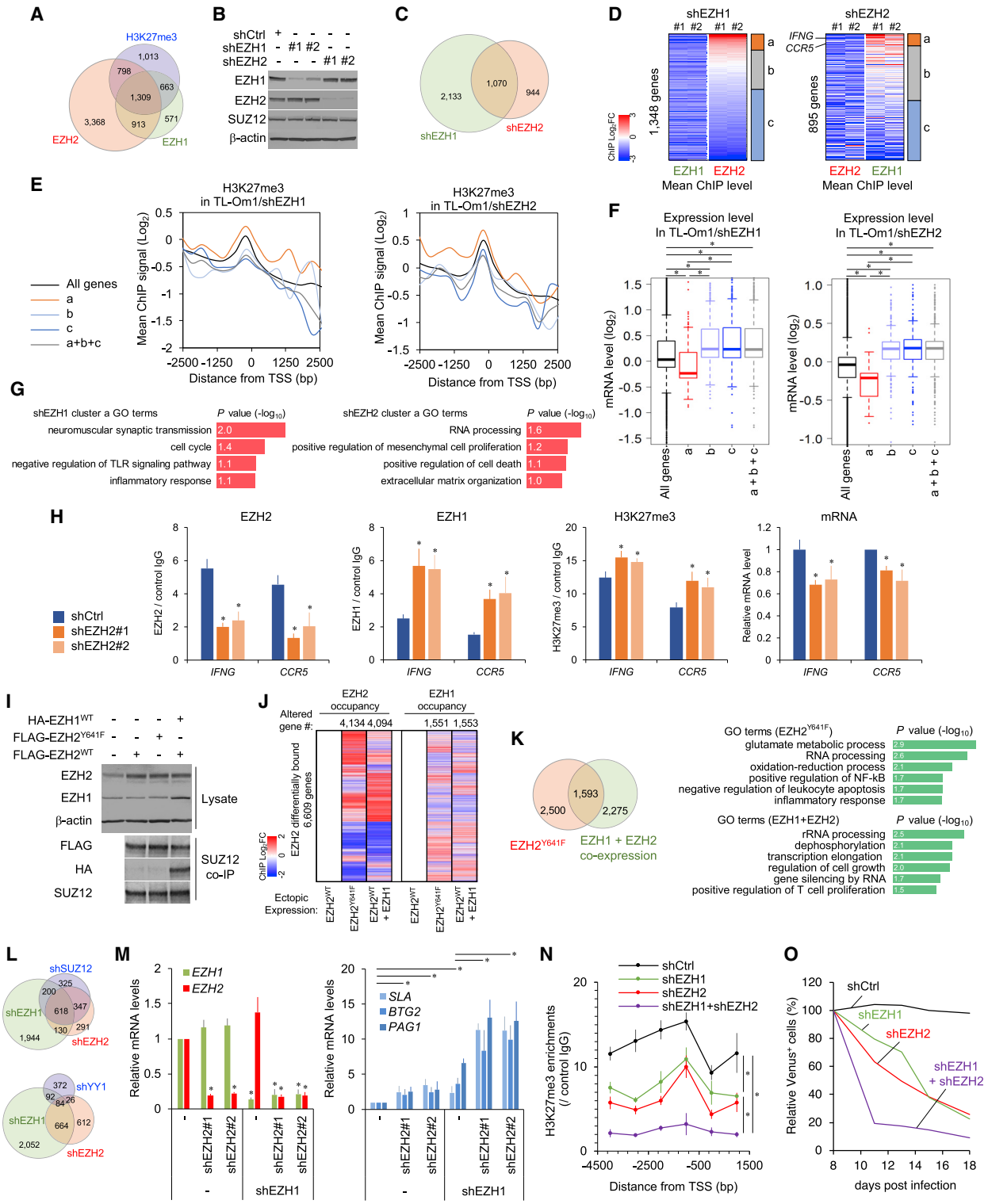

Figure 2. Reciprocal Function of EZH1 and EZH2

(A) Gene sets associated with H3K27me3, EZH1, and EZH2 in TL-Om1 cells.

(B) EZH1 and EZH2 levels in KD cells.

(C) H3K27me3-downregulated genes by EZH1 and EZH2 KD (H3K27me3 ChIP FC < −2 versus shCtrl).

(D) EZH1/2 chromatin distributions. The distribution patterns of EZH1 and EZH2 divided in three clusters.

(legend continued on next page)

characteristics. The experimental conditions of chromatin immunoprecipitation (ChIP) were confirmed at the representative H3K27me3 target (Yamagishi et al., 2012) (Figures S2F and S2G). Using this method, we analyzed occupancy of EZH1, EZH2, H3K27me3, and H3K4me3 at all gene transcription start sites (TSSs) in freshly isolated malignant cells of patients with acute ATL (n = 3) and normal $CD4^+$ T cells (n = 3). The mean ChIP signals of all genes showed deposition of H3K27me3, EZH1, and EZH2 in ATL cells compared with normal T cells (Figure 1E). Clustering analyses identified EZH1 and EZH2 target genes (Figure 1F). The ChIP data summary is shown in Figure 1G. More than 80% of TSS H3K27me3 upregulation was directly associated with the *cis* binding of EZH1 (29.1%), EZH2 (14.2%), or both (39.9%). ChIP peak analysis revealed H3K27me3 accumulation of the EZH1/2 target genes (Figures 1H, S2H, and S2I). Integration of transcriptome data (acute ATL, n = 26; normal $CD4^+$, n = 21) showed that abnormal binding of EZH1 and EZH2 caused transcriptional silencing (Figure 1I).

We also analyzed the methylation status of DNA CpG sites (>850,000 sites) in the same clinical cases and examined the relationship between promoter mCpG and H3K27me3. We detected many differentially methylated sites in ATL cells (7,408 hypermethylated sites [β value fold change (FC) > 0.2, $p < 0.05$, 4.54%], 6,925 hypomethylated sites [β value (FC) < −0.2, $p < 0.05$, 4.24%]) (Figure 1J). CpG methylation status of the H3K27me3-accumulated genes was relatively low in normal cells but significantly methylated in ATL cells (1,138 hypermethylated sites [13.1%] versus 226 hypomethylated sites [2.60%]), suggesting that chromatin condensation is cooperated by mCpG and EZH1/2-dependent H3K27me3 (Figure 1J).

Gene Ontology (GO) analysis revealed that EZH1- and EZH2-bound silenced genes involved various cellular processes (Figure 1K), including co-occupancy of EZH1 and EZH2 to silence multiple genes associated with transcriptional regulation, proliferation process, immune response, and cell migration. EZH1 would further directly induce H3K27me3 at genes involved with the regulation of lymphocyte activation and differentiation. EZH2 was specifically involved in various processes, including cellular metabolism, kinase regulation, and cytokine-mediated signaling. Principal-component analysis (PCA) revealed that all clinical subtypes showed epigenetic suppression of EZH1/2 targets (Figures 1L and S2J). Taken together, both EZH1 and EZH2 are important for the epigenetic landscape.

Reciprocal Function of EZH1 and EZH2

Despite the absence of quantitative change, genome-wide rearrangement of EZH1 was preferentially observed at promoters where the EZH2 binding pattern also changed (Figure 1G). To elucidate the mechanism of action of PRC2, we used ATL-derived TL-Om1 cells, which are dependent on EZH1/2 (Figures 1A and 2A). Specific shRNAs were used to establish EZH1- and EZH2-KD cells (Figure 2B). ChIP peak comparison detected H3K27me3 reduction in both KD cells (Figure 2C). The different effects on H3K27me3 suggested specific functions of the responsible enzymes. ChIP peak analysis of EZH1/2 chromatin distributions detected KD-mediated removal from TSS regions (Figure 2D). The distribution pattern of another enzyme corresponded to the depleted enzymes, which resulted in three potential clusters: reciprocal upregulation (cluster a), no change (cluster b), and cooperative downregulation (cluster c). To examine the functional significance of EZH1/2 redeployment, H3K27me3 levels were compared. KD of EZH1 and EZH2 generally reduced H3K27me3 (Figure 2E, a+b+c) and at cooperatively downregulated regions (clusters b and c). In contrast, reciprocal upregulation of another enzyme caused higher H3K27me3 (cluster a). The histone modification changes modulated transcription pattern. EZH KD and H3K27me3 reduction generally induced active transcription. However, the reciprocal upregulation of H3K27me3 caused transcription silencing (Figure 2F). The compensated genes are functional in several processes, such as cell death, cell cycle, and inflammatory response (Figure 2G). The epigenetic compensation was observed at representative loci in another cell line (Figure 2H). Thus, chromatin occupancy by EZH1 and EZH2 is critical for H3K27me3 and transcription patterns.

To test whether the EZH1/2 binding patterns are mutually interfered with each other, we ectopically expressed FLAG-tagged $EZH2^{WT}$, $EZH2^{Y641F}$ mutant (Morin et al., 2010; Béguelin et al., 2013), or $EZH2^{WT}$ with HA-tagged EZH1 in MCF7 breast cancer cells. Immunoblots of cell lysates and SUZ12-bound complex showed elevated expression of EZH1 and EZH2, which were effectively incorporated in PRC2 (Figure 2I). ChIP peak analysis showed that EZH1 and EZH2 were redistributed when both were co-expressed or EZH2 was mutated (Figure 2J). Co-expression of EZH1 and EZH2 generated new EZH1/2 occupied loci (3,868 genes), which were partially overlapped with the targets induced by EZH2 mutation (Figure 2K). Thus, the co-existence of EZH1-PRC2 and EZH2-PRC2 triggers an abnormal epigenetic pattern and affects several functional processes.

Transcriptome analysis identified gene sets highly sensitive to KD and indicated unique functions of EZH1/2 in gene regulation (Figure 2L), which was consistent with the results of the cell growth assay and the chromatin analysis. KD of the PRC2 components SUZ12 and YY1 (Simon and Kingston, 2009) are

(E and F) Mean H3K27me3 ChIP levels (E) and expression levels (F) of each cluster or all genes in TL-Om1 with shEZH1 (left) or shEZH2 (right). *$p < 0.01$.
(G) GO analysis of cluster a.
(H) Epigenetic pattern and mRNA level at cluster a genes in ATN-1 cells with shEZH2. n = 3, mean ± SD, *$p < 0.05$.
(I and J) $EZH2^{WT}$, $EZH2^{Y641F}$, and EZH1+$EZH2^{WT}$ were ectopically expressed in MCF7. Functional PRC2 was confirmed by SUZ12 co-IP (I). ChIP patterns of the EZH2-differentially bound genes (EZH2 ChIP abs(FC) > 4) are shown (J).
(K) EZH1 and/or EZH2 gain gene sets (left) and results of GO analysis (right).
(L) Upregulated gene sets (expression FC > 2 versus shCtrl).
(M–O) TL-Om1 cells were transduced with retro- and lenti-viruses expressing shEZH1 and shEZH2/Venus. Expression levels of *EZH1*, *EZH2*, and EZH1/2 targets (M; n = 3, mean ± SD, *$p < 0.05$), H3K27me3 level at *SLA* TSS (N; n = 3, mean ± SD, *$p < 0.05$), and results as Venus-competitive assay (O; representative of n = 2) are shown.
See also Figure S3.

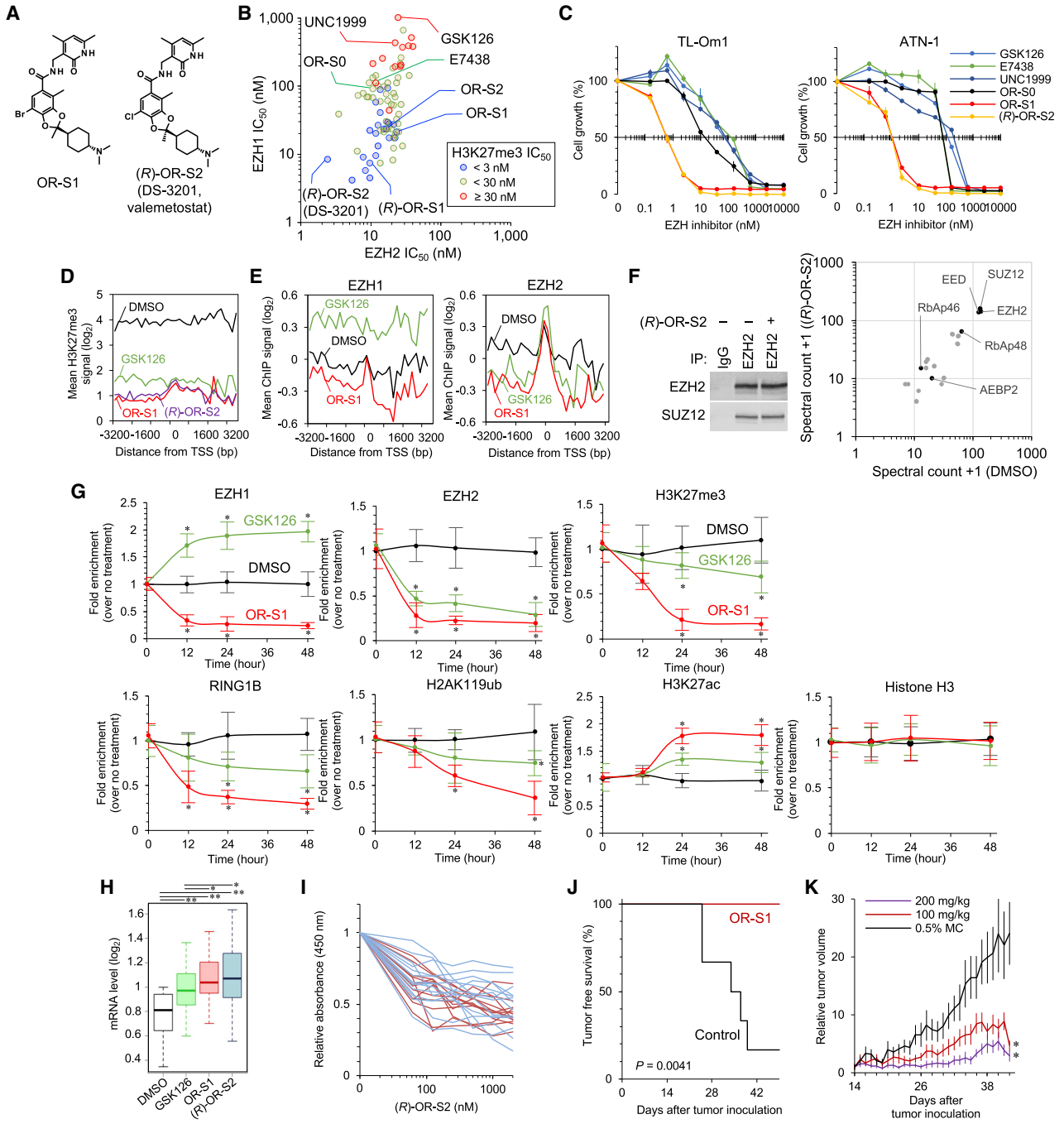

Figure 3. Chemical Dual Targeting of EZH1 and EZH2 in ATL

(A) Structures of EZH1/2 dual inhibitors.

(B) IC_{50} values of PRC2-EZH2 (x axis) and PRC2-EZH1 (y axis) of EZH inhibitors and their derivatives are plotted. Cell-based H3K27me3 reduction activities are indicated by colors.

(C) ATL cell lines were cultured for 14 days with several dose EZH inhibitors. Dose-dependent effects on cell growth (%) are shown. n = 3, mean ± SD.

(D) Mean H3K27me3 of top 1,000 genes in TL-Om1 cells treated with DMSO, GSK126 (1,000 nM), OR-S1 (100 nM), or (*R*)-OR-S2 (100 nM) for 7 days. Averaged peak data from biological duplicates are shown.

(E) Mean EZH1 and EZH2 values at OR-S1 targets 3,082 genes (100 nM OR-S1 H3K27me3 FC < −2 versus 1,000 nM GSK126).

(F) Endogenous EZH2-IP with whole-cell lysates from TL-Om1 cells in the presence or absence of 100 nM (*R*)-OR-S2 (DS-3201b). Proteins bound to the bait were identified by immunoblotting (left) and LC-MS/MS (right). Representative of n = 2 biological replicates.

(legend continued on next page)

partially involved in gene silencing, implying that the direct inhibition of enzymes is required for effective epigenetic reprogramming. Considering the overlapped localization and function, EZH1 and EZH2 were simultaneously depleted. Compared with single KD, EZH1/2 double KD significantly reactivated the EZH1/2 co-bound targets (Figure 2M). ChIP-PCR showed that H3K27me3 was significantly reduced by double KD (Figure 2N). The double-depleted ATL cells showed significantly reduced cell growth (Figure 2O). Collectively, EZH1 and EZH2 cooperatively form epigenetic and expression patterns, reflecting the growth of lymphoma cells.

Function of EZH1 under EZH2 Inhibition Condition

Although EZH1 compensates for the genetic deletion of *Ezh2* in embryonic stem cells (Shen et al., 2008), the role of EZH1 under the condition of EZH2 inhibition in somatic cells has not been addressed. Standard dose treatment with the EZH2-selective inhibitors GSK126 (McCabe et al., 2012) and E7438 (also called EPZ-6438 or tazemetostat [Knutson et al., 2014]) diminished H3K27me3 to a great extent, but residual methylation was detected (Figure S3A), which is consistent with the results of previous studies (McCabe et al., 2012; Fujikawa et al., 2016). The GSK126-treated cells showed robust H3K27me3 downregulation at 964 TSSs but also non-negligible H3K27me3 upregulation at 534 TSSs (Figure S3B). The focal H3K27me3 upregulation was concomitant with increased EZH1 occupancy and decreased gene expression (Figure S3C). Enzymatic inhibition caused removal of EZH2; however, EZH1 redeployment rapidly occurred at the EZH2-depleted or EZH1/2-free loci, where removal of H3K27me3 and gene reactivation were not achieved (Figures S3C and S3D). Time course ChIP-PCR validated the compensation of EZH1 (Figure S3E). EZH1 depletion effectively removed the residual H3K27me3 and significantly enhanced the efficacy of EZH2 inhibition, reflecting gene reactivation and cell growth inhibition (Figures S3F–S3I). Of note, DNA sequence suggested that YY1 may be partly involved in the EZH1/2 recruitment and their compensatory function (Figure S3D). YY1 KD attenuated the compensation of EZH1 in response to EZH2 inhibition, suggesting that compensatory action is partially mediated by YY1 (Figures S3J and S3K). Collectively, effective removal of H3K27me3 from $EZH2^{WT}$ cells can be accomplished by dual targeting of EZH1/2.

Chemical Dual Targeting of EZH1/2 in ATL

We previously conducted chemical screening and derivatization of EZH inhibitors with the use of the half maximal inhibitory concentration (IC_{50}) of EZH1/2 and cellular H3K27me3 (Honma et al., 2017). In particular, OR-S1 and (*R*)-OR-S2 (also called DS-3201 or valemetostat) strongly and specifically inhibited EZH1 and EZH2, respectively ($IC_{50} \leq 10$ nM) (Figure 3A). This selectivity was also profiled with the use of panels of 34 histone methyltransferases and 253 human protein kinases (Honma et al., 2017). To investigate the biological relevance and directly compare existing EZH inhibitors, unified experimental conditions for chemical synthesis and evaluation are required. For this purpose, we synthesized the EZH2-selective inhibitors E7438, GSK126, OR-S0 (Honma et al., 2017) and the EZH1/2 dual inhibitors OR-S1, (*R*)-OR-S2/DS-3201, and UNC1999 (Xu et al., 2015a) in house according to the chemical structures for this study (official IC_{50} values are shown in Figure S4A). The IC_{50} values against PRC2-EZH2 and PRC2-EZH1 were determined *in vitro*. In addition, cell-based H3K27me3 reduction activities were also examined. We found that the EZH1/2 dual inhibitors OR-S1 and OR-S2 had stronger activities as S-adenosyl-L-methionine (SAM)-competitive inhibitors (Figure 3B). The IC_{50} values of H3K27me3 were highly correlated with that of EZH1 (y axis), demonstrating that EZH1 inhibition is critical for H3K27me3 reduction under conditions of EZH2 inhibition. Therefore, the anti-growth activities of several compounds (annotated in Figure 3B) were tested in an *in vitro* dose escalation study, which showed that the EZH1/2 dual inhibitors significantly reduced ATL cell viability compared with the others (Figure 3C; growth inhibition activity fold change 136.8, range 29.5–273.0). Differential effects between OR-S1/2 and UNC1999 were correlated with the measured IC_{50} value against EZH1.

We performed ChIP peak analysis for H3K27me3, EZH1, and EZH2 and showed that the dual inhibitors effectively removed H3K27me3 and also prevented unexpected gain of H3K27me3 compared with a 10-fold dose of the EZH2 inhibitor (Figures 3D and S4B). OR-S1 effectively evicted both EZH1 and EZH2 at the downstream and upstream of the H3K27me3 sites (Figure 3E). In contrast, GSK126 treatment removed EZH2 only but led to a significant gain of EZH1 occupancy ($p < 10^{-88}$). Liquid chromatography-tandem mass spectrometry (LC-MS/MS) analysis of isolated complex by anti-EZH2 antibody showed no significant difference of PRC2 core components under treatment with dual inhibitors (Figure 3F). Thus, OR-S1/2 act as SAM-competitive inhibitors without complex disruption. Time course ChIP-PCR validated the removal of EZH1, EZH2, and H3K27me3 and also revealed reprogramming of the PRC1 component RING1B and its enzymatic product H2AK119ub and active chromatin mark H3K27ac by treatment with low-dose OR-S1 (Figure 3G). To obtain a global view of the impact

(G) Time course ChIP assay at *SLA* loci. TL-Om1 cells were treated with DMSO, 1,000 nM GSK126, or 100 nM OR-S1. ChIP-qPCR was conducted at 0, 12, 24, and 48 h after drug treatment. Data are shown as fold enrichment of means ± SD for six regions near the TSS; *$p < 0.05$.
(H) Expression levels of EZH1/2 target genes (H3K27me3 ChIP FC < -2 by OR-S1/2) in TL-Om1 treated with DMSO, GSK126 (1,000 nM), OR-S1 (100 nM), or (*R*)-OR-S2 (100 nM). Means of biological replicates n = 2. *$p < 10^{-14}$ and **$p < 10^{-71}$.
(I) Primary ATL cells (acute ATL, red lines, n = 12; chronic ATL, blue lines, n = 14) were cultured for 7 days in the presence of several dose of EZH inhibitors. Residual cell numbers were analyzed using WST-8 assay. Details are provided in Figure S4I.
(J) NOD/SCID mice inoculated with TL-Om1 were orally administered with OR-S1 (200 mg/kg, daily, n = 6) or 0.5% methylcellulose (n = 6). Kaplan-Meier curve shows tumor-free survival (p value: nonparametric log rank test).
(K) After tumor engraftment (at day 14), OR-S1 were orally administered daily. Relative tumor volumes are shown (n = 6 or 7, mean ± SEM, *$p < 0.05$).
See also Figures S4 and S5.

of EZH1/2 dual inhibition, we analyzed ChIP signals at the H3K27me3 downregulated 4,610 genes. The occupancy of EZH2 and the compensatory redistribution of EZH1 were effectively inhibited, and these initial changes were further accompanied by the removal of H2AK119ub, feedback increase of H3K27ac and H3K4me3, and recruitment of RNA polymerase II (Figures 3E and S4C). Expression analysis revealed global reactivation of H3K27me3-accumulated genes. The dual inhibitors significantly reduced H3K27me3 and effectively reactivated the expression of EZH1/2 targets compared with 10-fold dose of GSK126 (Figures 3H and S4D–S4F). These results demonstrated that EZH1/2 inhibition effectively reprogrammed the epigenomic abnormalities.

We further sought to ascertain the effects of dual inhibitors in two more biological models. Dual inhibitor treatment significantly reactivated the expression of the highly H3K27me3-accumulated EZH1/2 target genes in an *ex vivo* culture of primary ATL cells (Figures S4G and S4H). The treatment reduced the viability of all tested ATL cells more effectively than the EZH2 inhibitor (Figures 3I and S4I). Furthermore, oral administration of OR-S1 completely prevented ATL cell engraftment and *in vivo* growth in immunodeficient mice (Figures 3J, 3K, and S4J–S4L). We confirmed significant inhibition of tumor growth and liver metastasis, without significant body weight loss. These data indicate that EZH1/2 dual inhibitors have strong potential for anti-ATL activity.

Integrative transcriptome and epigenome data identified epigenetic silencing of functionally important genes (Figure S5A). EZH1/2 inhibitors effectively diminished H3K27me3 and induced gene reactivation (Figures S5B and S5C). The gene set includes *SLA* and *PAG1* as CD3ζ (*CD247*)-T cell receptor (TCR) signal negative regulators (Smida et al., 2007; Érsek et al., 2012), *BTG1* and *BTG2* tumor suppressors (Winkler, 2010), *TBX21*, *CCR5* for lineage specification, and *EMP1* and *HEG1* for cell-cell junction (Kleaveland et al., 2009). The dual inhibitors significantly induced *SLA* and *PAG1*, disrupting cell surface CD3ζ, which is critical for TCR signaling pathway (Brownlie and Zamoyska, 2013) and may be linked to strong apoptosis (Figures S5C–S5E).

Hyperactive EZH1/2 have also been implicated in the silencing of NF-κB negative regulators (Yamagishi et al., 2012) and are suggested to associate directly with NF-κB components (Lee et al., 2011). Dual inhibitors significantly upregulated H3K27me3-accumulated microRNAs, removed RelA, RelB, and acetylated histones from NF-κB target loci, and prevented target gene expression (Figures S5F–S5K). Cellular NF-κB deactivation was achieved by low-dose EZH1/2 inhibitors (Figure S5L).

Furthermore, continuous inhibition (1 week) of EZH1/2 resulted in significant alterations of RNA polymerase II occupancy and transcriptome without H3K27me3 changes (Figure S5M), which may have resulted from the effects of reprogramming of multiple transcription factors (Figure 1K). Thus, malignant cells have a complex transcriptome network that is initially established by EZH1/2. Collectively, inhibitor-dependent H3K27me3 downregulation directly and indirectly reprograms the transcriptome, explaining the effectiveness of the EZH1/2 dual inhibitors.

Dual Targeting of EZH1/2 in Malignant Lymphomas

We next probed the cell sensitivity to the dual inhibitors using a panel of malignant lymphoma cell lines that originated from $EZH1^{+}$ differentiated lymphocytes, including peripheral T cell lymphoma (PTCL; including ATL), diffuse large B cell lymphoma (DLBCL; $EZH2^{WT/WT}$ and $EZH2^{WT/Mu}$), Burkitt lymphoma (BL), and primary effusion lymphoma (PEL). All of the tested models showed considerable miR-31 silencing, suggesting abnormal H3K27me3 deposition (Figure S5N). In addition, *MLL*-rearranged leukemia was also tested because previous studies showed high sensitivity to EZH1/2 inhibitors (Neff et al., 2012; Xu et al., 2015a; Honma et al., 2017). To directly compare the growth IC_{50} values, we performed *in vitro* dose escalation study and determined IC_{50} values of GSK126, OR-S1, and (*R*)-OR-S2 (DS-3201) by the unified experimental condition. We found superior anti-growth effects of the dual inhibitors compared with EZH2-selective inhibitor in all models (Figure 4A; growth inhibition activity fold change 29.3, range 4.99–417.9). All calculated IC_{50} values were less than 1,000 nM, suggesting that malignant lymphomas and *MLL*-rearranged leukemia are generally sensitive to the EZH1/2 inhibitors. (*R*)-OR-S2 potently inhibited H3K27me3 by low-dose treatment (0.1–100 nM) in the sensitive lymphoma types, demonstrating on-target effects (Figure 4B).

Rank ordering particularly indicated that ATL and other T cell-derived lymphomas are highly sensitive to EZH1/2 inhibitors. PTCL is a category of malignancies with poor prognosis that are derived from mature T cells, for which no durable molecular targeting therapy has been established (Vose et al., 2008). We re-analyzed previous transcriptome data from clinical PTCL cases (n = 141; Iqbal et al., 2010) and found stable expression of *EZH1* and overexpression of *EZH2* in all types of PTCL, including PTCL-NOS, AITL, and ALCL (Figure 4C). Overexpression of EZH2 is mediated by several transcription factors, including NF-κB (Fujikawa et al., 2016). We found that TCR/CD28 pathway is critical for EZH1/2 expression (Figure 4D). Short-term activation was insufficient to achieve the stable EZH2 overexpression, suggesting the requirement of constitutive activation of the TCR pathway, which is frequently detected in T cell lymphomas (Kataoka et al., 2015; Vallois et al., 2016). Indeed, inhibition of NF-κB reduced *EZH2* expression in all PTCL cell lines (Figure 4E). EZH1 was stably and highly expressed and was not affected by NF-κB inhibition.

Further inspection of clinical cases revealed that all PTCL subtypes showed decreased expression of the EZH1/2 target genes, involving cell growth and other functional processes (Figure 1), and were differentially clustered from normal lymphocytes, suggesting that T cell-derived lymphoma has EZH1/2-dependent epigenetic changes (Figures 4F, 4G, and S5O). The EZH1/2 dual inhibitors showed superior anti-growth effects compared with EZH2-selective inhibitors and UNC1999 in PTCL models (Figure 4H), as well as in *MLL*-rearranged leukemia models (Figure 4I). These results suggest that T cell lymphoma is a primary disease category for treatment with EZH1/2 inhibitors.

Cell line-based screening also suggested that germinal center (GC)-type and non-GC-type DLBCL are also potential disease entities. We collected clinical frozen samples and found that DLBCL cells highly expressed both *EZH1* and *EZH2* (Figure 5A). *EZH2* baseline level was low and significantly upregulated in

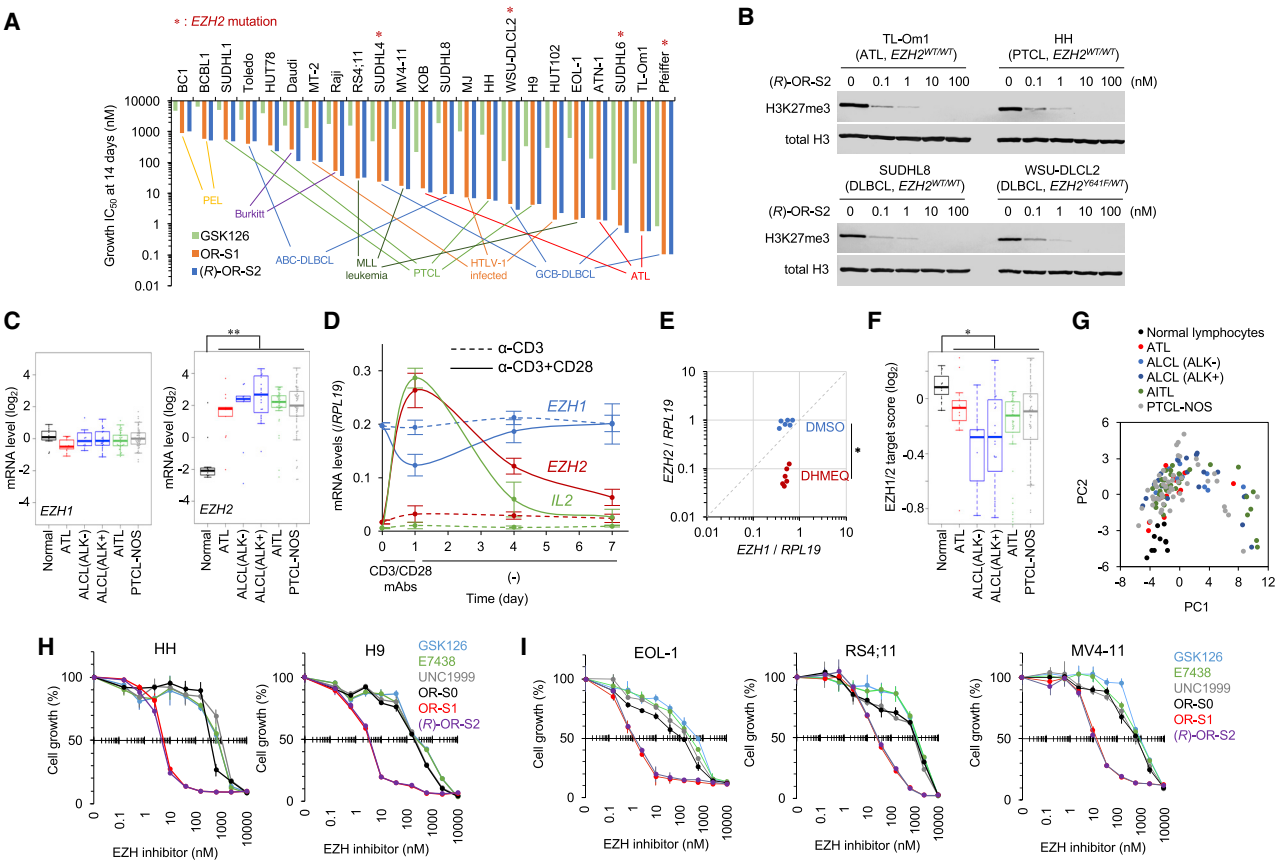

Figure 4. Targeting EZH1 and EZH2 in Malignant Lymphomas

(A) The effect of OR-S1, (*R*)-OR-S2, and GSK126 on 23 cell lines derived from hematological malignancies represented as the concentrations required to inhibit 50% of growth after 14 days. Means of n = 3 biological replicates; statistical significance between OR-S1/2 and GSK126 was observed in all models. *EZH2* mutation is indicated by asterisk.

(B) Evaluation of H3K27me3 in four sensitive cell lines following treatment for 7 days.

(C) *EZH1* and *EZH2* levels in PTCL cohort (normal lymphocytes, n = 11; ATL, n = 13; ALK[−]-anaplastic large cell lymphoma (ALCL), n = 10; ALK[+]-ALCL, n = 20; angioimmunoblastic T cell lymphoma [AITL], n = 37; peripheral T cell lymphoma, not other specified [PTCL-NOS], n = 50). **p < 0.001.

(D) Expression changes by transient TCR signal in $CD4^+$ T cells. Cells were washed at day 1 and maintained without monoclonal antibodies (mAbs) for 7 days. n = 3, mean ± SD.

(E) Six T cell lymphoma cells were treated with DHMEQ (5 μg/mL) for 24 h. Quantified *EZH1* and *EZH2* were plotted. n = 3, *p < 0.05.

(F) Averaged levels of EZH1/2 target 307 genes (H3K27me3 ChIP FC > 2, expression FC < −2, EZH1 and/or EZH2 ChIP FC > 0 in ATL cells versus normal T cells) in PTCL cohort. *p < 0.02.

(G) PCA clustering on the basis of expression data of EZH1/2 target genes.

(H and I) PTCL (H) and MLL-fusion leukemia (I) cell lines were cultured for 14 days in the presence of several dose EZH inhibitors. n = 3, mean ± SD.

See also Figure S5.

DLBCL, although there was no statistical significance among clinical subtypes (GC versus non-GC, Epstein-Barr virus [EBV]− versus EBV+), suggesting that EZH1/2 expression is a common characteristic. Another DLBCL cohort (Tagawa et al., 2005) validated high expression levels (Figure S5P). As is the case with T cell lymphoma, DLBCL is frequently associated with hyper-activation of immune receptor signaling. We found that the proximal promoter sequence was significantly activated by B cell receptor (BCR) engagement (Figure 5B). In addition, mimetic models of BCR pathway activation, including mutations to *CARD11* (Lenz et al., 2008) and *MYD88* (Ngo et al., 2011), as well as inactivation of A20 (Kato et al., 2009; Compagno et al., 2009) and PTEN (Mayo et al., 2002; Perkins, 2012), showed enhanced promoter activity, suggesting that *EZH2* may be over-expressed in the majority of malignant B cells (Figure 5C).

Some DLBCL cases (~21.7% of GCB-DLBCL) have heterozygous *EZH2* mutation (Morin et al., 2010). To unravel the molecular mechanism underlying the H3K27me3 accumulation with EZH1 and EZH2, we selected two cell models harboring $EZH2^{WT/WT}$ (SUDHL8) or $EZH2^{Y641F/WT}$ (WSU-DLCL2); the latter type is sensitive to EZH2 inhibition (Figure 4A). shRNA-mediated KD showed that EZH2 was essential for both models. In contrast, EZH1 KD was critical for $EZH2^{WT/WT}$ cells but not for $EZH2^{Y641F/WT}$ cells (Figure 5D). We next tested the sensitivity of DLBCL cells to the EZH2 inhibitor in the presence or absence of shEZH1. In addition to $EZH2^{WT/WT}$ cells, $EZH2^{Y641F/WT}$ cells

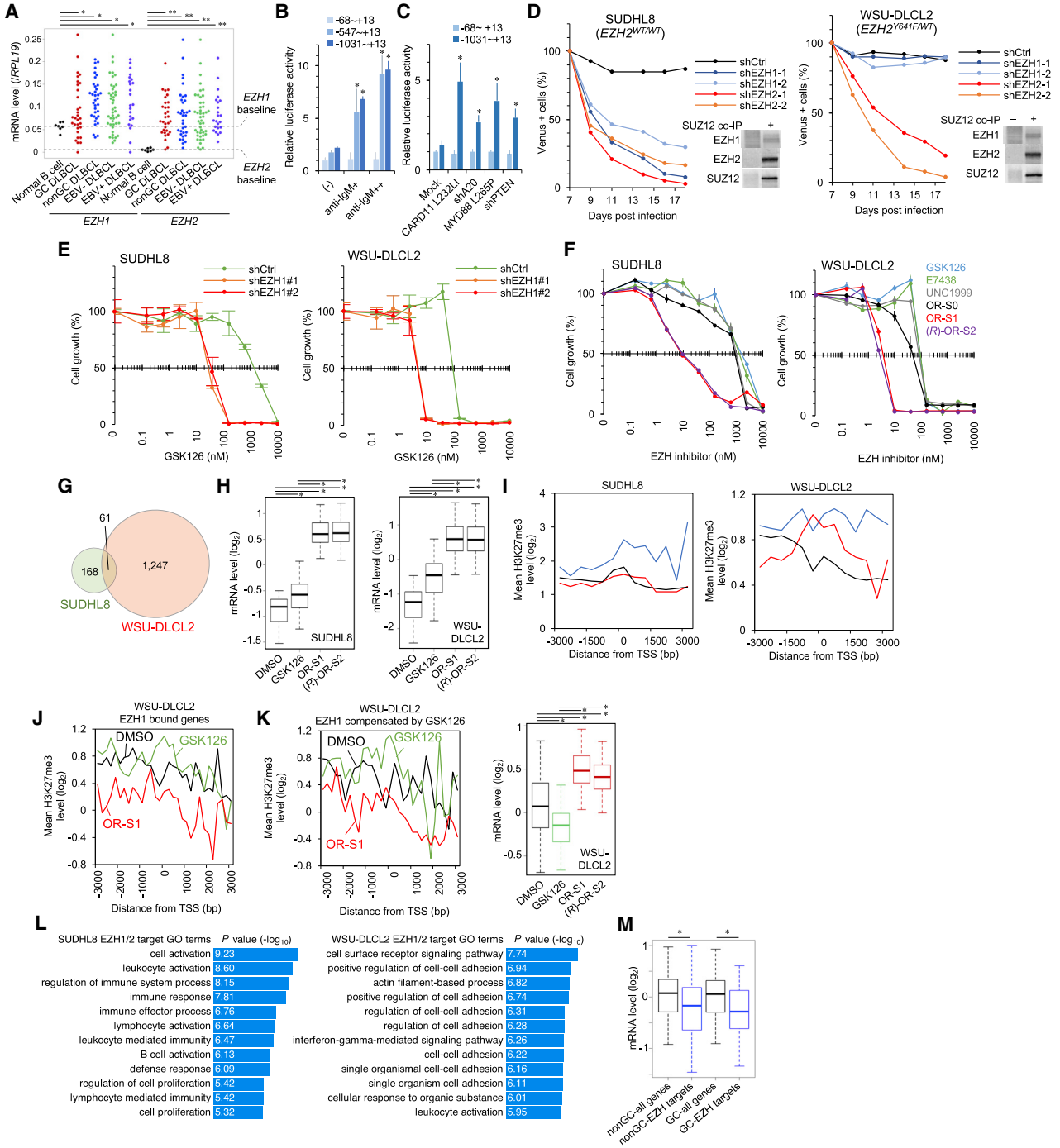

Figure 5. EZH1- and EZH2-Dependent H3K27me3 in DLBCL

(A) *EZH1* and *EZH2* levels in primary frozen DLBCL (GC, n = 31; non-GC, n = 35; EBV[−], n = 45; EBV[+], n = 23) and $CD19^+$ normal B cells (n = 7). *$p < 0.01$ and **$p < 10^{-7}$.

(B) *EZH2* promoter activity in BJAB cells treated with anti-IgM. n = 4, mean ± SD, *$p < 0.05$.

(C) *EZH2* promoter activity in BCR pathway-activating cells. n = 4, mean ± SD, *$p < 0.05$.

(D) SUDHL8 (non-GC type, $EZH2^{WT/WT}$, $BCL6^-/CD10^-$) and WSU-DLCL2 (GC type, $EZH2^{WT/Y641F}$, $BCL6^+/CD10^+$) were treated with shEZH1 or shEZH2, and results as Venus-competitive assay (representative of n = 2) are shown. Functional PRC2 was detected by SUZ12 co-IP.

(E) SUDHL8 and WSU-DLCL2 with shCtrl or shEZH1 (#1, #2) were cultured for 14 days in the presence of several dose GSK126. n = 3, mean ± SD.

(F) DLBCL cell lines were cultured for 14 days in the presence of several dose EZH inhibitors. n = 3, mean ± SD.

(legend continued on next page)

showed high sensitivity upon EZH1 depletion, suggesting a compensatory action of EZH1 upon EZH2 inhibition regardless of the *EZH2* mutation status (Figure 5E). Consistent with above mechanism, EZH1/2-targeting H3K27me3 inhibition and synthetic lethality were confirmed in both cell types (Figures 4B and 5F). The superior effect of EZH1/2 dual inhibition was further confirmed in all tested B cell malignancies (DLBCL, BL, and PEL) with both $EZH2^{WT/WT}$ (six lines) and $EZH2^{Mu/WT}$ (four lines) (Figure 4A).

We further explored whole expression data and identified genotype-specific dual-inhibitor-responsive gene sets (Figures 5G and 5H). $EZH2^{Y641F/WT}$ cells showed high sensitivity at gene reactivation level. ChIP peak analysis after inhibitor treatment revealed that the gene set was under the control of H3K27me3, and OR-S1 could reduce methylation to baseline levels (Figure 5I). Treatment with OR-S1, but not GSK126, diminished H3K27me3 at the EZH1 targets (Figure 5J). Furthermore, GSK126 also induced substantial methylation compensation with bound EZH1, but OR-S1 reduced H3K27me3 significantly and reactivated the expression (Figure 5K), suggesting that EZH1 inhibition is critical for targeting DLBCL epigenome. GO analysis suggested that EZH1/2 was involved in the regulation of the several functional processes, such as cell growth and activation and the immune response, explaining the effective growth inhibition in both types (Figure 5L). Finally, the transcriptome data of primary cases showed that the expression levels of the EZH1/2 targets were significantly low in both the non-GC and GC types of DLBCL (Figures 5M and S5Q). Collectively, DLBCL may also be responsive to EZH1/2 inhibitors.

Synthetic Lethality Targeting Various Cancer Epigenome

We next examined the relationship between EZH1/2-mediated histone methylation and chromatin remodeling in heterochromatin formation. mSWI/SNF (BAF complex) is one of the most frequently mutated chromatin remodeling genes in a wide variety of cancers (Hodges et al., 2016), in which EZH2 activity has been implicated (Wilson et al., 2010; Bitler et al., 2015; Kim et al., 2015; Yamagishi and Uchimaru, 2017). We found antagonistic functions of both EZH1 and EZH2 to BAF. Dual depletion or dual inhibition of EZH1/2 induced rapid recruitment of the BAF components ARID1A, BRG1 (*SMARCA4*), and SNF5 (*SMARCB1*), accessible chromatin formation, and stable transcription (Figures 6A–6D). Prolonged treatment (7 days) further enhanced chromatin accessibility and gene expression, suggesting that effective epigenetic reprogramming requires long-time exposure.

Genome-wide promoter analysis demonstrated global BAF pattern changes and the opposite reactions of BAF and EZH1/2 (Figures 6E and 6F). Chromatin unwinding effectively occurred upon EZH1/2 dual inhibition, which induced changes of expression (Figures 6G and 6H). The opposite action was observed in the heterochromatin formation process; namely, hyper-activation of EZH1/2 was associated with BAF eviction (Figure 6I). Conversely, BAF depletion globally recruited both EZH1 and EZH2 and silenced transcription, which could be canceled by EZH1/2 inhibition (Figures 6J–6N). These data support the notion that, in addition to EZH2, EZH1 plays a critical role in BAF-mediated chromatin remodeling.

Gene mutations of other epigenetic factors are strongly associated with cancers such as *KDM6A* (H3K27 demethylase) and *BAP1* (histone H2A deubiquitinase), which are implicated in H3K27me3-dependent cancers (Ler et al., 2017; LaFave et al., 2015). We analyzed all the promoter regions in *KDM6A*- and *BAP1*-KD cells and found EZH1- and EZH2-dependent H3K27me3 accumulation, which could be canceled by OR-S1 treatment (Figures 7A–7D). Expression profiling identified common target genes, including Th1-type chemokines, leading to innate immune evasion (Peng et al., 2015) (Figures 7E and 7F). These data suggest that inactivation of the EZH1/2 antagonists have oncogenic roles with H3K27me3 accumulation in various cancers. Indeed, ARID1A-KD, KDM6A-KD, and BAP1-KD cells showed high sensitivity to OR-S1 (Figure 7G). The strong synthetic lethality was induced when both EZH1 and EZH2 were inhibited. Furthermore, an *in vitro* dose escalation study showed higher antiproliferation activity of the dual inhibitors than the EZH2 inhibitor in cell models of *SMARCB1* (SNF5)-mutated malignant rhabdoid tumors (G-401), *ARID1A*-mutated ovarian clear cell carcinoma (TOV-21G), and *BAP1*-mutated mesothelioma (NCI-H226) (Figure 7H).

The epigenetic balance between H3K27me3 and H3K4me3 is a main determinant of transcription (Schuettengruber et al., 2007; Piunti and Shilatifard, 2016). In particular, the MLL2-containing trithorax group regulates H3K4 methylation, and *MLL2* (*KMT2D*) is frequently inactivated in B cell lymphomas (Pasqualucci et al., 2011; Morin et al., 2011). Analysis of primary samples revealed that *MLL2* transcription was silenced in DLBCL (Figure 7I). Depletion of the *MLL2* genes promoted EZH1/2-dependent cell growth in pre-tumorigenic EBV+ B cell lymphoblastoid (LCL) cells (Figures 7J and 7K). *MLL2* loss led to H3K4me3 loss at 2,322 gene promoters, whereas concomitant H3K27me3 gain was observed in 1,402 genes (60.4%) with *cis* bindings of EZH1 and/or EZH2 (Figures 7L and 7M).

These findings suggest that the facultative heterochromatin formation involves both EZH1/EZH2 and chromatin remodeling

(G–I) SUDHL8 and WSU-DLCL2 cells were treated with GSK126 (1,000 nM), OR-S1 (100 nM), or (*R*)-OR-S2 (100 nM) for 7 days. Gene expression profiling identified dual-inhibitor-responsive gene sets (expression FC > 2 by OR-S1/2, *p < 10^{-15}). Gene numbers (G) and expression levels (H) are shown. Mean H3K27me3 ChIP values of all genes (black), the inhibitor-responsive gene set with DMSO (blue) or OR-S1 (red) near the TSS are shown (I).

(J) Mean H3K27me3 ChIP values of EZH1 target 894 genes (EZH1 ChIP FC < −1.5 by 100 nM OR-S1) in WSU-DLCL2 cells treated with EZH inhibitors.

(K) Mean H3K27me3 ChIP values (left) and gene expression (right) of EZH1 compensated 495 genes (EZH1 ChIP FC > 2 by 1,000 nM GSK126).

(L) Gene Ontology ($-\log_{10}$[p value]) of the dual-inhibitor-responsive gene sets.

(M) Expression levels of all genes versus EZH1/2 target genes (expression FC > 2 by EZH1/2 inhibitors in WSU-DLCL2 and SUDHL8) in primary GC- and non-GC-DLBCL cells. *p < 0.01.

See also Figure S5.

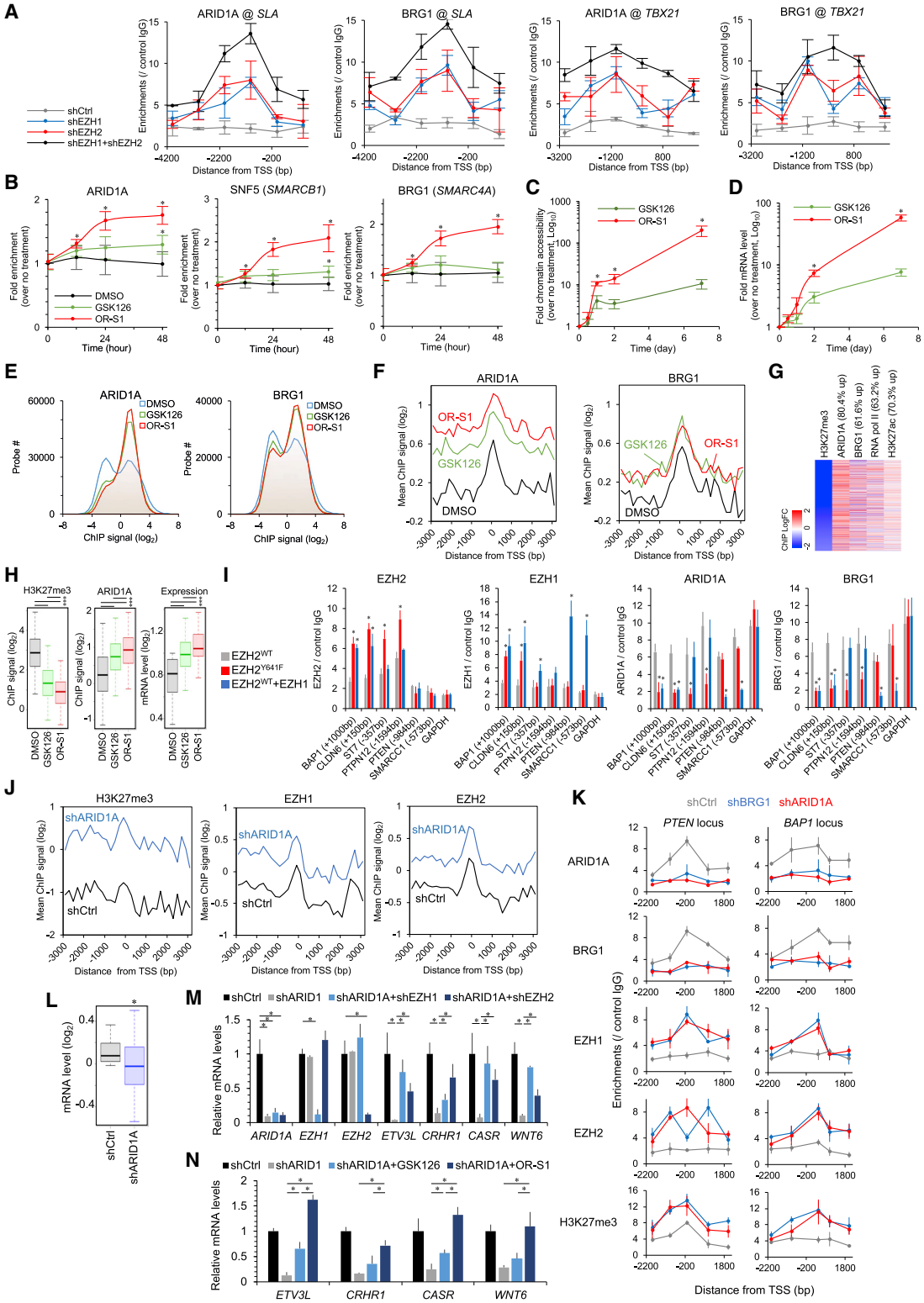

Figure 6. Importance of EZH1 and EZH2 in BAF-Mutated Cancers

(A) Chromatin occupancy of ARID1A and BRG1 in TL-Om1 with shEZH1 and/or shEZH2. n = 3, mean ± SD, $p < 0.05$ between single-KD versus double-KD was observed.

(legend continued on next page)

factors in (1) aberrant EZH1 + EZH2 dual-expressing tumors, like the majority of lymphomas; (2) EZH2 GoF mutated DLBCL and follicular lymphoma (FL); and (3) other cancer types with mutations in epigenetic factor genes, which are suggested to occur in early clonal evolution (Flavahan et al., 2017) (Figure 7N). The inactivation of genes involved in chromatin relaxation (H3K27 demethylation, H3K4 trimethylation, H2A deubiquitination, and chromatin unwinding) caused restricted H3K27me3 accumulation mediated by both EZH1 and EZH2, which may be an emerging vulnerable characteristic in certain cancer types. Large numbers of regulated genes are unique in each epigenetic pathway of cancers.

Targeting Epigenetic Changes of Premalignant Cells

Besides genetic and expression changes of epigenetic factors, oncovirus infection may be one of the initial drivers of epigenetic changes. We reanalyzed the transcriptome data from asymptomatic individuals or indolent-type ATL patients and detected EZH1- and EZH2-dependent epigenetic silencing at a part of the target loci in the human T-lymphotropic virus 1 (HTLV-1)-infected cells (Figures S6A–S6D). EZH1/2 inhibition diminished abnormal methylation with EZH1/2 removal in a Tax-expressing HTLV-1-infected cell model (Figures S6E and S6F). In addition, H3K27me3 ChIP peak from Tax-dependent immortalized T cells (Fujikawa et al., 2016) showed that H3K27me3 was upregulated at both EZH1 and EZH2 targets (Figure S6G). Higher antiproliferation activity of the dual inhibitors compared with EZH2-selective inhibitors was detected in the HTLV-1-infected cell lines (Figure 4A). To further test whether EZH1/2 dual inhibition can selectively deplete the HTLV-1-infected cell population, we conducted low-dose treatment of OR-S1 and OR-S2/DS-3201 in primary *ex vivo* culture. EZH1/2 inhibitors selectively depleted the HTLV-1-infected cell population in indolent ATL patients (11 of 13 [84.6%]) and asymptomatic carriers (31 of 35 [88.6%]) more effectively than a 5-fold dose of the EZH2-selective inhibitor (Figures S6H–S6J). These data suggest that targeting of EZH1 and EZH2 is an effective strategy to diminish the HTLV-1-infected cell population.

EBV is a B cell-tropic oncovirus, which influences the host epigenome (Allday, 2013; Jiang et al., 2017). We found that EBV-infected LCLs expressed both EZH1 and EZH2, and the cell proliferation was highly dependent on both EZH1 and EZH2 (Figures S7A and S7B). Transcriptome and epigenome analyses revealed EZH1- and EZH2-dependent global H3K27me3 redistribution in EBV-infected, untransformed cells (Figures S7C–S7E). EZH1/2 inhibition significantly affected the transcriptome, which contributed to the several functional processes (Figures S7F–S7I). In contrast, low-dose did not affect cell death and the proliferation of normal lymphocytes *in vitro* (Figures S7J and S7K). These data collectively suggest that two lymphotropic oncoviruses, HTLV-1 and EBV, reprogrammed the global EZH1/2-H3K27me3 patterns and established the unique transcriptome in the non-malignant, virus-infected cell population.

DISCUSSION

Precise target molecule(s) should be identified for mechanism-based medicine. EZH2 has been recognized as the molecule responsible for excessively accumulated H3K27 methylation, which is one of the molecular hallmarks of cancers, because of GoF mutation and/or overexpression of EZH2.

In this study, we discovered the involvement of another enzyme, EZH1, in abnormal H3K27 methylation. We showed that the chromatin distribution of EZH1 is globally reprogrammed and tightly involved in the global histone methylation in aggressive lymphomas. Reciprocal interference and compensatory action of the EZH1 and EZH2 rearrange their own genome-wide distribution, establishing restricted chromatin and gene expression signatures.

On the basis of these findings, we developed EZH1+EZH2 dual inhibitors (among them, valemetostat/DS-3201b has been used in clinical trials) and demonstrated significant H3K27me3 inhibition efficacy. LC-MS/MS showed that the SAM-competitive dual inhibitors do not alter PRC2 core complex composition, but chromatin occupancy of EZH1 and EZH2 are decreased, which may potentiate and sustain the drug effect. Considering that trimethylated H3K27 itself is an active interaction site of PRC2 and stimulates PRC2 activity (Margueron et al., 2009), one possible mechanism is that diminishment of trimethylation mark might lead to weak interaction with PRC2.

In exploring mechanisms of action of the inhibitors, we also showed that both EZH1 and EZH2 play critical roles in the chromatin regulation together with multiple histone modifiers and chromatin regulatory factors. Strong synthetic lethality was observed in cancer cells harboring mutations to histone-modifying genes, as well as in pre-cancerous cells epigenetically perturbed by oncovirus infection. In addition to EZH1/2 dysregulation, inactivation of genes involved in chromatin relaxation and

(B–D) Time course epigenetic alteration at *SLA* loci. TL-Om1 cells were treated with DMSO, 1,000 nM GSK126, or 100 nM OR-S1. ChIP assay were conducted for 48 h (B). Time course evaluation of chromatin accessibility (C; n = 3) and transcription (D; n = 3) were also conducted for 7 days. Mean ± SD, *p < 0.05.
(E and F) TL-Om1 cells were treated with EZH inhibitors for 7 days. Normalized all ChIP signals (E) and mean values of ARID1A and BRG1 at H3K27me3 decreased 3,086 loci (F) are shown.
(G) Epigenetic reprogramming by 100 nM OR-S1 treatment at H3K27me3 decreased loci.
(H) H3K27me3 (left) and ARID1A (middle) ChIP values and expression levels of EZH1/2 target genes (right). *p < 10^{-15}.
(I) MCF7 cells were transfected with FLAG-EZH2^{WT}, FLAG-EZH2^{Y641F}, or FLAG-EZH2^{WT} + HA-EZH1. Promoter binding pattern at EZH1/2 targets and *GDPDH* loci was analyzed using ChIP-PCR assay. n = 3, mean ± SD, *p < 0.05 versus EZH2^{WT} expression.
(J) MCF7/shARID1A were analyzed using ChIP-chip. EZH1 and EZH2 recruitments at H3K27me3 upregulated loci (H3K27me3 FC > 2 by ARID1A KD, 2,376 genes) were induced by ARID1A KD.
(K) Epigenetic patterns at *PTEN* and *BAP1* loci. n = 3, mean ± SD.
(L) Expression levels of H3K27me3 upregulated genes. *p < 10^{-36}.
(M and N) Expression levels of ARID1A-EZH1/2 targets. Gene silencing induced by ARID1A KD was canceled by shEZH1 and shEZH2 (M) or 100 nM OR-S1 (N). n = 3, mean ± SD, *p < 0.05.

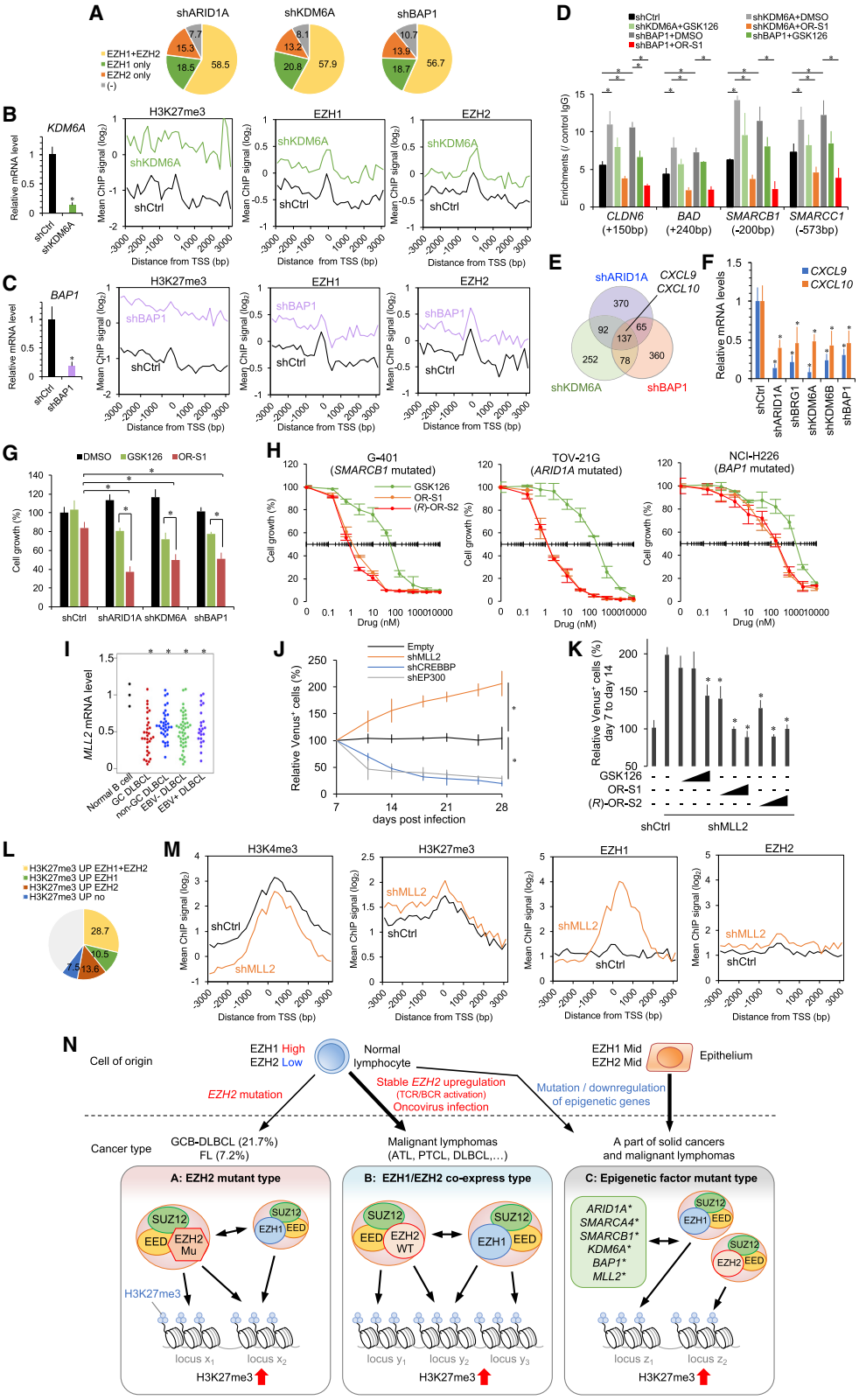

(legend on next page)

virus infection appear to be vulnerable characteristics (Figure 7N). Further clinical epigenomics in primary tumors by using high-sensitive assays may be helpful to establish mechanism-based medicine and develop accurate biomarkers.

Regarding the diversity of genetic lesions in lymphomas, the developmental pathway seems to be initiated by EZH1/2 and epigenetically imprinted in the non-malignant, virus-infected population throughout disease development. This finding could provide new preemptive therapeutic strategies for the elimination of malignant cells and their founder population in human malignancies. Repeated dosing did not cause any critical or severe toxicity *in vitro* and *in vivo* (Honma et al., 2017), suggesting that (pre)malignant cells are more highly addicted by EZH1/2-dependent epigenome than normal cells.

This study provides convincing rationale for dual targeting of EZH1+EZH2 and suggests the validity of drugs for treating malignant lymphomas and premalignant clones. On the basis of these results, a phase 1 clinical trial against T- and B cell non-Hodgkin's lymphomas including ATL is now under way, and clinical safety and promising activity against lymphomas have been suggested (Maruyama et al., 2018, Am. Soc. Hematol., conference).

STAR★METHODS

Detailed methods are provided in the online version of this paper and include the following:

- KEY RESOURCES TABLE
- LEAD CONTACT AND MATERIALS AVAILABILITY
- EXPERIMENTAL MODEL AND SUBJECT DETAILS
  - Cell culture
  - Clinical samples
  - Chemicals
- METHOD DETAILS
  - Cell-free assay to detect methyltransferase activities
  - Cell-based assay to detect H3K27me3 reduction
  - Liquid chromatography-tandem mass spectrometry (LC-MS/MS)
  - Flow cytometry
  - Chromatin immunoprecipitation (ChIP) assay
  - Chromatin accessibility assay
  - RNA isolation and RT-PCR analysis
  - Vectors
  - NF-κB analysis
  - Immunoblotting and immunoprecipitation
  - Quantification of HTLV-1 proviral load
  - Cell growth assay
  - *In vivo* xenograft studies
  - ChIP-chip experiments
  - Gene expression analysis
  - DNA methylation analysis
  - GEO gene expression data
- QUANTIFICATION AND STATISTICAL ANALYSIS
- DATA AND CODE AVAILABILITY

SUPPLEMENTAL INFORMATION

Supplemental Information can be found online at https://doi.org/10.1016/j.celrep.2019.10.083.

ACKNOWLEDGMENTS

We thank staff members at all collaborating institutions and the central office of the JSPFAD. We thank Drs. Hiroyuki Miyoshi and Atsushi Miyawaki for providing the Venus-encoding lentivirus vectors. We thank Dr. Kazuo Umezawa for providing the NF-κB inhibitor DHMEQ. This research was supported by AMED under grants JP18ak0101086 (M.Y., K.U., T.W.), JP17fk0108112 (K.U., T.W.), JP17im0210101 (K.U., K.A.), and JP17fk0410208 (K.U., S.O., H.K.) and JSPS KAKENHI grants JP15K06907 (M.Y.), JP16H05323 (M.Y), and JP18K08317 (M.Y).

AUTHOR CONTRIBUTIONS

M.Y. conceived and supervised the project; designed and performed almost all experiments, including the gene expression profile, ChIP experiments, *in vitro* cell culture, and drug evaluation; performed data analysis; and wrote the paper. M.H. performed ChIP-chip for EZH1 and EZH2 in ATL clinical samples. D.F. established the ChIP-chip experiments and supervised data analysis. T.O. performed *in vivo* studies. D.H. and N.A. produced EZH1/2 inhibitors and analyzed chemical properties. H.K. and T.H. prepared DLBCL clinical samples and provided advice. S.K. and K.N. developed the CADM1/CD7-based flow cytometry method, provided clinical samples, and obtained gene expression data. M.N. prepared ATL clinical samples. M.I. maintained the JSPFAD and analyzed epidemiological data. A.U. provided clinical samples and gave advice. Y.T. provided anti-Tax antibody. S.O. organized DLBCL study and provided advice. K. Tsukasaki and K. Tobinai managed ATL clinical study and provided advice. K.A. managed the EZH1/2 dual inhibitor project and provided advice. T.W. established the ATL cohort study and supervised

Figure 7. Importance of EZH1 and EZH2 in *KDM6A*, *BAP1*, and *MLL2* Mutated Cancer Types

(A–C) Proportion of EZH1/2-bindings at H3K27me3 gain genes triggered by depletion of *ARID1A* (2,369 genes), *KDM6A* (2,509 genes), and *BAP1* (2,219 genes) (A). KD efficiencies and mean ChIP values at H3K27me3 upregulated loci are shown (B and C). n = 3, mean ± SD, *p < 0.05.

(D) MCF7/shCtrl, /shKDM6A, and /shBAP1 were treated with EZH inhibitors for 7 days, and H3K27me3 were quantified. n = 3, mean ± SD, *p < 0.05.

(E) Gene sets downregulated by depletion of *ARID1A*, *KDM6A*, and *BAP1* (expression FC < −2).

(F) *CXCL9* and *CXCL10* levels. n = 3, mean ± SD, *p < 0.05.

(G) Cell growth (%) at day 14 treated with EZH inhibitors. n = 3, mean ± SD, *p < 0.05.

(H) Dose-dependent effects on cell growth (%) for 14 days. n = 3, mean ± SD.

(I) *MLL2* mRNA level in DLBCL samples. *p < 0.05.

(J) Venus-competitive assay in LCLs transduced with shRNA lentivirus vectors. n = 3, mean ± SD, *p < 0.05.

(K) LCL/shMLL2 cells were treated with EZH inhibitors (10, 100, and 1,000 nM). $Venus^+$ rate (day 7 to day 14) is shown. n = 3, mean ± SD, *p < 0.05 versus shMLL2 without inhibitors.

(L) *MLL2* depletion led to H3K4me3 loss at 2,322 genes in LCL. Proportion of concomitant H3K27me3 gain (60.4%) with *cis* bindings of EZH1/2 is shown.

(M) Mean ChIP values at H3K4me3 downregulated loci (H3K4me3 FC < −1.5 in MLL2 KD cells, 2,322 genes).

(N) A schematic view illustrating modes of H3K27me3 accumulation.

See also Figures S6 and S7.

the ATL study. K.U. conceived and supervised the project and wrote the paper. All authors discussed the results and commented on the manuscript.

DECLARATION OF INTERESTS

D.H., N.A., and K.A. are employees of Daiichi Sankyo Co., Ltd. M.Y. and K.U. received research funding from Daiichi Sankyo Co., Ltd. Daiichi Sankyo Co., Ltd., holds substance patents on the EZH1/2 inhibitors. The University of Tokyo and Daiichi Sankyo Co., Ltd., hold patents for application of the EZH1/2 inhibitors to ATL patients and HTLV-1-infected individuals. M.Y., T.W., D.H., and N.A. are named as inventors. All other authors declare no competing interests.

Received: April 1, 2019
Revised: September 8, 2019
Accepted: October 21, 2019
Published: November 19, 2019

REFERENCES

Allday, M.J. (2013). EBV finds a polycomb-mediated, epigenetic solution to the problem of oncogenic stress responses triggered by infection. Front. Genet. *4*, 212.

Béguelin, W., Popovic, R., Teater, M., Jiang, Y., Bunting, K.L., Rosen, M., Shen, H., Yang, S.N., Wang, L., Ezponda, T., et al. (2013). EZH2 is required for germinal center formation and somatic EZH2 mutations promote lymphoid transformation. Cancer Cell *23*, 677–692.

Bitler, B.G., Aird, K.M., Garipov, A., Li, H., Amatangelo, M., Kossenkov, A.V., Schultz, D.C., Liu, Q., Shih, IeM., Conejo-Garcia, J.R., et al. (2015). Synthetic lethality by targeting EZH2 methyltransferase activity in ARID1A-mutated cancers. Nat. Med. *21*, 231–238.

Bradley, W.D., Arora, S., Busby, J., Balasubramanian, S., Gehling, V.S., Nasveschuk, C.G., Vaswani, R.G., Yuan, C.C., Hatton, C., Zhao, F., et al. (2014). EZH2 inhibitor efficacy in non-Hodgkin's lymphoma does not require suppression of H3K27 monomethylation. Chem. Biol. *21*, 1463–1475.

Brownlie, R.J., and Zamoyska, R. (2013). T cell receptor signalling networks: branched, diversified and bounded. Nat. Rev. Immunol. *13*, 257–269.

Cao, R., and Zhang, Y. (2004). SUZ12 is required for both the histone methyltransferase activity and the silencing function of the EED-EZH2 complex. Mol. Cell *15*, 57–67.

Comet, I., Riising, E.M., Leblanc, B., and Helin, K. (2016). Maintaining cell identity: PRC2-mediated regulation of transcription and cancer. Nat. Rev. Cancer *16*, 803–810.

Compagno, M., Lim, W.K., Grunn, A., Nandula, S.V., Brahmachary, M., Shen, Q., Bertoni, F., Ponzoni, M., Scandurra, M., Califano, A., et al. (2009). Mutations of multiple genes cause deregulation of NF-kappaB in diffuse large B-cell lymphoma. Nature *459*, 717–721.

Érsek, B., Molnár, V., Balogh, A., Matkó, J., Cope, A.P., Buzás, E.I., Falus, A., and Nagy, G. (2012). CD3ζ-chain expression of human T lymphocytes is regulated by TNF via Src-like adaptor protein-dependent proteasomal degradation. J. Immunol. *189*, 1602–1610.

Flavahan, W.A., Gaskell, E., and Bernstein, B.E. (2017). Epigenetic plasticity and the hallmarks of cancer. Science *357*, eaal2380.

Fujikawa, D., Nakagawa, S., Hori, M., Kurokawa, N., Soejima, A., Nakano, K., Yamochi, T., Nakashima, M., Kobayashi, S., Tanaka, Y., et al. (2016). Polycomb-dependent epigenetic landscape in adult T-cell leukemia. Blood *127*, 1790–1802.

Hans, C.P., Weisenburger, D.D., Greiner, T.C., Gascoyne, R.D., Delabie, J., Ott, G., Müller-Hermelink, H.K., Campo, E., Braziel, R.M., Jaffe, E.S., et al. (2004). Confirmation of the molecular classification of diffuse large B-cell lymphoma by immunohistochemistry using a tissue microarray. Blood *103*, 275–282.

Hodges, C., Kirkland, J.G., and Crabtree, G.R. (2016). The many roles of BAF (mSWI/SNF) and PBAF complexes in cancer. Cold Spring Harb. Perspect. Med. *6*, a026930.

Honma, D., Kanno, O., Watanabe, J., Kinoshita, J., Hirasawa, M., Nosaka, E., Shiroishi, M., Takizawa, T., Yasumatsu, I., Horiuchi, T., et al. (2017). Novel orally bioavailable EZH1/2 dual inhibitors with greater antitumor efficacy than an EZH2 selective inhibitor. Cancer Sci. *108*, 2069–2078.

Iqbal, J., Weisenburger, D.D., Greiner, T.C., Vose, J.M., McKeithan, T., Kucuk, C., Geng, H., Deffenbacher, K., Smith, L., Dybkaer, K., et al.; International Peripheral T-Cell Lymphoma Project (2010). Molecular signatures to improve diagnosis in peripheral T-cell lymphoma and prognostication in angioimmunoblastic T-cell lymphoma. Blood *115*, 1026–1036.

Italiano, A., Soria, J.C., Toulmonde, M., Michot, J.M., Lucchesi, C., Varga, A., Coindre, J.M., Blakemore, S.J., Clawson, A., Suttle, B., et al. (2018). Tazemetostat, an EZH2 inhibitor, in relapsed or refractory B-cell non-Hodgkin lymphoma and advanced solid tumours: a first-in-human, open-label, phase 1 study. Lancet Oncol. *19*, 649–659.

Iwanaga, M., Watanabe, T., Utsunomiya, A., Okayama, A., Uchimaru, K., Koh, K.R., Ogata, M., Kikuchi, H., Sagara, Y., Uozumi, K., et al.; Joint Study on Predisposing Factors of ATL Development investigators (2010). Human T-cell leukemia virus type I (HTLV-1) proviral load and disease progression in asymptomatic HTLV-1 carriers: a nationwide prospective study in Japan. Blood *116*, 1211–1219.

Jiang, S., Zhou, H., Liang, J., Gerdt, C., Wang, C., Ke, L., Schmidt, S.C.S., Narita, Y., Ma, Y., Wang, S., et al. (2017). The Epstein-Barr virus regulome in lymphoblastoid cells. Cell Host Microbe *22*, 561–573.e4.

Kataoka, K., Nagata, Y., Kitanaka, A., Shiraishi, Y., Shimamura, T., Yasunaga, J., Totoki, Y., Chiba, K., Sato-Otsubo, A., Nagae, G., et al. (2015). Integrated molecular analysis of adult T cell leukemia/lymphoma. Nat. Genet. *47*, 1304–1315.

Kato, M., Sanada, M., Kato, I., Sato, Y., Takita, J., Takeuchi, K., Niwa, A., Chen, Y., Nakazaki, K., Nomoto, J., et al. (2009). Frequent inactivation of A20 in B-cell lymphomas. Nature *459*, 712–716.

Katsuya, H., Yamanaka, T., Ishitsuka, K., Utsunomiya, A., Sasaki, H., Hanada, S., Eto, T., Moriuchi, Y., Saburi, Y., Miyahara, M., et al. (2012). Prognostic index for acute- and lymphoma-type adult T-cell leukemia/lymphoma. J. Clin. Oncol. *30*, 1635–1640.

Kim, K.H., Kim, W., Howard, T.P., Vazquez, F., Tsherniak, A., Wu, J.N., Wang, W., Haswell, J.R., Walensky, L.D., Hahn, W.C., et al. (2015). SWI/SNF-mutant cancers depend on catalytic and non-catalytic activity of EZH2. Nat. Med. *21*, 1491–1496.

Kleaveland, B., Zheng, X., Liu, J.J., Blum, Y., Tung, J.J., Zou, Z., Sweeney, S.M., Chen, M., Guo, L., Lu, M.M., et al. (2009). Regulation of cardiovascular development and integrity by the heart of glass-cerebral cavernous malformation protein pathway. Nat. Med. *15*, 169–176.

Knutson, S.K., Warholic, N.M., Wigle, T.J., Klaus, C.R., Allain, C.J., Raimondi, A., Porter Scott, M., Chesworth, R., Moyer, M.P., Copeland, R.A., et al. (2013). Durable tumor regression in genetically altered malignant rhabdoid tumors by inhibition of methyltransferase EZH2. Proc. Natl. Acad. Sci. U S A *110*, 7922–7927.

Knutson, S.K., Kawano, S., Minoshima, Y., Warholic, N.M., Huang, K.C., Xiao, Y., Kadowaki, T., Uesugi, M., Kuznetsov, G., Kumar, N., et al. (2014). Selective inhibition of EZH2 by EPZ-6438 leads to potent antitumor activity in EZH2-mutant non-Hodgkin lymphoma. Mol. Cancer Ther. *13*, 842–854.

Kobayashi, S., Nakano, K., Watanabe, E., Ishigaki, T., Ohno, N., Yuji, K., Oyaizu, N., Asanuma, S., Yamagishi, M., Yamochi, T., et al. (2014). CADM1 expression and stepwise downregulation of CD7 are closely associated with clonal expansion of HTLV-I-infected cells in adult T-cell leukemia/lymphoma. Clin. Cancer Res. *20*, 2851–2861.

Kundaje, A., Meuleman, W., Ernst, J., Bilenky, M., Yen, A., Heravi-Moussavi, A., Kheradpour, P., Zhang, Z., Wang, J., Ziller, M.J., et al.; Roadmap Epigenomics Consortium (2015). Integrative analysis of 111 reference human epigenomes. Nature *518*, 317–330.

LaFave, L.M., Béguelin, W., Koche, R., Teater, M., Spitzer, B., Chramiec, A., Papalexi, E., Keller, M.D., Hricik, T., Konstantinoff, K., et al. (2015). Loss of BAP1 function leads to EZH2-dependent transformation. Nat. Med. *21*, 1344–1349.

Lee, S.T., Li, Z., Wu, Z., Aau, M., Guan, P., Karuturi, R.K., Liou, Y.C., and Yu, Q. (2011). Context-specific regulation of NF-κB target gene expression by EZH2 in breast cancers. Mol. Cell *43*, 798–810.

Lenz, G., Davis, R.E., Ngo, V.N., Lam, L., George, T.C., Wright, G.W., Dave, S.S., Zhao, H., Xu, W., Rosenwald, A., et al. (2008). Oncogenic CARD11 mutations in human diffuse large B cell lymphoma. Science *319*, 1676–1679.

Ler, L.D., Ghosh, S., Chai, X., Thike, A.A., Heng, H.L., Siew, E.Y., Dey, S., Koh, L.K., Lim, J.Q., Lim, W.K., et al. (2017). Loss of tumor suppressor KDM6A amplifies PRC2-regulated transcriptional repression in bladder cancer and can be targeted through inhibition of EZH2. Sci. Transl. Med. *9*, eaai8312.

Margueron, R., Li, G., Sarma, K., Blais, A., Zavadil, J., Woodcock, C.L., Dynlacht, B.D., and Reinberg, D. (2008). Ezh1 and Ezh2 maintain repressive chromatin through different mechanisms. Mol. Cell *32*, 503–518.

Margueron, R., Justin, N., Ohno, K., Sharpe, M.L., Son, J., Drury, W.J., 3rd, Voigt, P., Martin, S.R., Taylor, W.R., De Marco, V., et al. (2009). Role of the polycomb protein EED in the propagation of repressive histone marks. Nature *461*, 762–767.

Mayo, M.W., Madrid, L.V., Westerheide, S.D., Jones, D.R., Yuan, X.J., Baldwin, A.S., Jr., and Whang, Y.E. (2002). PTEN blocks tumor necrosis factor-induced NF-κ B-dependent transcription by inhibiting the transactivation potential of the p65 subunit. J. Biol. Chem. *277*, 11116–11125.

McCabe, M.T., Ott, H.M., Ganji, G., Korenchuk, S., Thompson, C., Van Aller, G.S., Liu, Y., Graves, A.P., Della Pietra, A., 3rd, Diaz, E., et al. (2012). EZH2 inhibition as a therapeutic strategy for lymphoma with EZH2-activating mutations. Nature *492*, 108–112.

Morin, R.D., Johnson, N.A., Severson, T.M., Mungall, A.J., An, J., Goya, R., Paul, J.E., Boyle, M., Woolcock, B.W., Kuchenbauer, F., et al. (2010). Somatic mutations altering EZH2 (Tyr641) in follicular and diffuse large B-cell lymphomas of germinal-center origin. Nat. Genet. *42*, 181–185.

Morin, R.D., Mendez-Lago, M., Mungall, A.J., Goya, R., Mungall, K.L., Corbett, R.D., Johnson, N.A., Severson, T.M., Chiu, R., Field, M., et al. (2011). Frequent mutation of histone-modifying genes in non-Hodgkin lymphoma. Nature *476*, 298–303.

Neff, T., Sinha, A.U., Kluk, M.J., Zhu, N., Khattab, M.H., Stein, L., Xie, H., Orkin, S.H., and Armstrong, S.A. (2012). Polycomb repressive complex 2 is required for MLL-AF9 leukemia. Proc. Natl. Acad. Sci. U S A *109*, 5028–5033.

Ngo, V.N., Young, R.M., Schmitz, R., Jhavar, S., Xiao, W., Lim, K.H., Kohlhammer, H., Xu, W., Yang, Y., Zhao, H., et al. (2011). Oncogenically active MYD88 mutations in human lymphoma. Nature *470*, 115–119.

Pasqualucci, L., Trifonov, V., Fabbri, G., Ma, J., Rossi, D., Chiarenza, A., Wells, V.A., Grunn, A., Messina, M., Elliot, O., et al. (2011). Analysis of the coding genome of diffuse large B-cell lymphoma. Nat. Genet. *43*, 830–837.

Peng, D., Kryczek, I., Nagarsheth, N., Zhao, L., Wei, S., Wang, W., Sun, Y., Zhao, E., Vatan, L., Szeliga, W., et al. (2015). Epigenetic silencing of TH1-type chemokines shapes tumour immunity and immunotherapy. Nature *527*, 249–253.

Perkins, N.D. (2012). The diverse and complex roles of NF-κB subunits in cancer. Nat. Rev. Cancer *12*, 121–132.

Pfister, S.X., and Ashworth, A. (2017). Marked for death: targeting epigenetic changes in cancer. Nat. Rev. Drug Discov. *16*, 241–263.

Piunti, A., and Shilatifard, A. (2016). Epigenetic balance of gene expression by Polycomb and COMPASS families. Science *352*, aad9780.

Qi, W., Chan, H., Teng, L., Li, L., Chuai, S., Zhang, R., Zeng, J., Li, M., Fan, H., Lin, Y., et al. (2012). Selective inhibition of Ezh2 by a small molecule inhibitor blocks tumor cells proliferation. Proc. Natl. Acad. Sci. U S A *109*, 21360–21365.

Schuettengruber, B., Chourrout, D., Vervoort, M., Leblanc, B., and Cavalli, G. (2007). Genome regulation by polycomb and trithorax proteins. Cell *128*, 735–745.

Shen, X., Liu, Y., Hsu, Y.J., Fujiwara, Y., Kim, J., Mao, X., Yuan, G.C., and Orkin, S.H. (2008). EZH1 mediates methylation on histone H3 lysine 27 and complements EZH2 in maintaining stem cell identity and executing pluripotency. Mol. Cell *32*, 491–502.

Simon, J.A., and Kingston, R.E. (2009). Mechanisms of polycomb gene silencing: knowns and unknowns. Nat. Rev. Mol. Cell Biol. *10*, 697–708.

Smida, M., Posevitz-Fejfar, A., Horejsi, V., Schraven, B., and Lindquist, J.A. (2007). A novel negative regulatory function of the phosphoprotein associated with glycosphingolipid-enriched microdomains: blocking Ras activation. Blood *110*, 596–615.

Tagawa, H., Suguro, M., Tsuzuki, S., Matsuo, K., Karnan, S., Ohshima, K., Okamoto, M., Morishima, Y., Nakamura, S., and Seto, M. (2005). Comparison of genome profiles for identification of distinct subgroups of diffuse large B-cell lymphoma. Blood *106*, 1770–1777.

Vallois, D., Dobay, M.P., Morin, R.D., Lemonnier, F., Missiaglia, E., Juilland, M., Iwaszkiewicz, J., Fataccioli, V., Bisig, B., Roberti, A., et al. (2016). Activating mutations in genes related to TCR signaling in angioimmunoblastic and other follicular helper T-cell-derived lymphomas. Blood *128*, 1490–1502.

Vose, J., Armitage, J., and Weisenburger, D.; International T-Cell Lymphoma Project (2008). International peripheral T-cell and natural killer/T-cell lymphoma study: pathology findings and clinical outcomes. J. Clin. Oncol. *26*, 4124–4130.

Wilson, B.G., Wang, X., Shen, X., McKenna, E.S., Lemieux, M.E., Cho, Y.J., Koellhoffer, E.C., Pomeroy, S.L., Orkin, S.H., and Roberts, C.W. (2010). Epigenetic antagonism between polycomb and SWI/SNF complexes during oncogenic transformation. Cancer Cell *18*, 316–328.

Winkler, G.S. (2010). The mammalian anti-proliferative BTG/Tob protein family. J. Cell. Physiol. *222*, 66–72.

Xu, B., On, D.M., Ma, A., Parton, T., Konze, K.D., Pattenden, S.G., Allison, D.F., Cai, L., Rockowitz, S., Liu, S., et al. (2015a). Selective inhibition of EZH2 and EZH1 enzymatic activity by a small molecule suppresses MLL-rearranged leukemia. Blood *125*, 346–357.

Xu, J., Shao, Z., Li, D., Xie, H., Kim, W., Huang, J., Taylor, J.E., Pinello, L., Glass, K., Jaffe, J.D., et al. (2015b). Developmental control of polycomb subunit composition by GATA factors mediates a switch to non-canonical functions. Mol. Cell *57*, 304–316.

Yamagishi, M., and Uchimaru, K. (2017). Targeting EZH2 in cancer therapy. Curr. Opin. Oncol. *29*, 375–381.

Yamagishi, M., Nakano, K., Miyake, A., Yamochi, T., Kagami, Y., Tsutsumi, A., Matsuda, Y., Sato-Otsubo, A., Muto, S., Utsunomiya, A., et al. (2012). Polycomb-mediated loss of miR-31 activates NIK-dependent NF-κB pathway in adult T cell leukemia and other cancers. Cancer Cell *21*, 121–135.

STAR★METHODS

KEY RESOURCES TABLE

REAGENT or RESOURCE	SOURCE	IDENTIFIER
Antibodies		
EZH2	Cell Signaling Technology	Cat# 3147S; RRID: AB_10694383
APC Mouse Anti-Human CD4, Clone RPA-T4	BD Biosciences	Cat# 555349; RRID: AB_398593
PE Mouse Anti-Human CD19, Clone HIB19	BD Biosciences	Cat# 555413; RRID: AB_395813
FITC Mouse Anti-human CD7, Clone CD7-6B7	Bio Legend	Cat# 343104; RRID: AB_1659216
FITC Mouse Anti-CD247 (TCRζ, CD3ζ), Clone 6B10.2	Bio Legend	Cat# 644103; RRID: 2244275
CADM1	MBL	Cat# CM005; RRID: 592782
Anti-H3K27me3	Millipore	Cat# 07-449; RRID: 310624
Anti-H3K4me3	Millipore	Cat# 07-473; RRID: 1977252
Anti-H3K27ac	Millipore	Cat# 07-360; RRID: 310550
Anti-EZH2	Millipore	Cat# 07-689; RRID: 417397
Anti-EZH1	Abcam	Cat# ab13665; RRID: 300546
Anti-RNA polymerase II	Active Motif	Cat# 39097; RRID: 2732926
Anti-normal Rabbit IgG	Cell Signaling Technology	Cat# 2729S; RRID: 1031062
Anti-SUZ12	Cell Signaling Technology	Cat# 3737S; RRID: 2196850
Anti-total histone H3	Abcam	Cat# ab10799; RRID: 470239
Anti-H2AK119ub	Millipore	Cat# 05-678; RRID: 309899
Anti-RING1B	Cell Signaling Technology	Cat# 5694S; RRID: 10705604
anti-ARID1A	Santa Cruz	Cat# sc-32761; RRID: 673396
Anti-SNF5	Abcam	Cat# ab12167; RRID: 298898
Anti-BRG1	Abcam	Cat# ab110641; RRID: 10861578
Anti-YY1	Santa Cruz	Cat# sc-1703; RRID: 2218501
Anti-RelA	Santa Cruz	Cat# sc-8008; RRID: 628017
Anti-RelB	Santa Cruz	Cat# sc-226; RRID: 632341
Anti-FLAG (M2)	Sigma-Aldrich	Cat# F1804; RRID: 262044
Anti-HA	MBL	Cat# 561; RRID: 591839
Anti-Tax (Lt-4)	Tanaka Y.	N/A
Anti-β-actin	Santa Cruz	Cat# sc-69879; RRID: 1119529
Anti-Mouse IgG (H+L), HRP Conjugate	Promega	Cat# W4021; RRID: 430834
Anti-Rabbit IgG (H+L), HRP Conjugate	Promega	Cat# W4011; RRID: 430833
Anti-CD3 pure - functional grade, human	Miltenyi Biotec	Cat# 130-093-387; RRID: 1036144
Anti-CD28 pure - functional grade, human	Miltenyi Biotec	Cat# 130-093-375; RRID: 1036134
F(ab')2 Fragment Goat Anti-Human IgM, Fc5mu Fragment Specific	Jackson Immunoresearch Laboratories	Cat# 109-006-129; RRID: 2337553
Chemicals, Peptides, and Recombinant Proteins		
(*R*)-OR-S2 (valemetostat, DS-3201)	Honma et al., 2017	N/A
OR-S1	Honma et al., 2017	N/A
OR-S0	Honma et al., 2017	N/A
GSK126	This study	N/A
E7438 (EPZ-6438, tazemetostat)	This study	N/A
UNC1999	This study	N/A
DHMEQ	Umezawa K.	N/A
Streptavidin-PE	Thermo Scientific	Cat# SA10041
biotin N-hydroxysuccinimide ester	Sigma-Aldrich	Cat# H1759

(*Continued on next page*)

Continued

REAGENT or RESOURCE	SOURCE	IDENTIFIER
Ficoll-Paque	GE Healthcare	Cat# 17144003
RPMI1640	Thermo Scientific	Cat# 11875093
Fetal bovine serum (FBS)	Thermo Scientific	Cat# 26140079
Dulbecco's Modified Eagle's Medium (DMEM)	Nissui	Cat# 05919
Penicillin Streptomycin	Thermo Scientific	Cat# 15140122
L-Glutamine	Thermo Scientific	Cat# 25030081
Recombinant human IL-2	R&D Systems	Cat# 202-IL
Adenosyl-L-methionine, S-[methyl-^{3}H] (SAM[^{3}H])	Perkin Elmer	Cat# NET155V
S-adenosyl-L-methionine (SAM)	New England BioLabs	Cat# B9003S
Biotinylated H3 peptide (residues 21-44)	AnaSpec	Cat# AS-64440-025
Streptavidin-coated FlashPlate	Perkin Elmer	Cat# SMP103
Micrococcal Nuclease (MNase)	New England BioLabs	Cat# M0247S
SYBR Select Master Mix	Thermo Scientific	Cat# 4472908
TRIzol	Thermo Scientific	Cat# 15596026
ISOGEN	Nippon gene	Cat# 311-02501
SuperScript II Reverse Transcriptase	Thermo Scientific	Cat# 18064014
Lipofectamine 2000	Thermo Scientific	Cat# 11668019
Critical Commercial Assays		
Annexin V Apoptosis Detection Kit PE	Thermo Scientific	Cat# 88-8102-72
Chromatin Accessibility Assay Kit	Abcam	Cat# ab185901
Cell Counting Kit-8	Dojindo	Cat# CK04
SurePrint G3 Human Promoter Microarray	Agilent Technologies	Cat# G4820A
4 × 44K Whole Human Genome Oligo Microarray	Agilent Technologies	Cat# G4845A
Infinium MethylationEPIC BeadChip	Illumina	Cat# WG-317
CD4^{+} T Cell Isolation Kit	Miltenyi Biotec	Cat# 130-096-533
B cell Isolation Kit II	Miltenyi Biotec	Cat# 130-091-151
AlphaLISA Tri-Methyl-Histone H3 Lysine 27 (H3K27me3) Cellular Detection Kit	Perkin Elmer	Cat# AL722
MicroRNA Assays	Thermo Scientific	Cat# A25576
Dual-Luciferase Reporter Assay System	Promega	Cat# E1910
RNeasy Mini Kit	QIAGEN	Cat# 74104
QIAamp DNA Blood Mini Kit	QIAGEN	Cat# 51106
Deposited Data		
Microarray data (gene expression)	This study	GEO: GSE138282
ChIP-on-chip data (epigenetic data)	This study	GEO: GSE138342
Experimental Models: Cell Lines		
TL-Om1	Sugamura K.	N/A
ATN-1	RIKEN	Cat# RCB1440
HH	ATCC	Cat# CRL-2105
H9	ATCC	Cat# HTB-176
MJ	ATCC	Cat# CRL-8294
RS4;11	ATCC	Cat# CRL-1873
MV4-11	ATCC	Cat# CRL-9591
G-401	ATCC	Cat# CRL-1441
TOV21G	ATCC	Cat# CRL-11730
NCI-H226	ATCC	Cat# CRL-5826
MCF7	ATCC	Cat# HTB-22

(*Continued on next page*)

Continued

REAGENT or RESOURCE	SOURCE	IDENTIFIER
HCT116	ATCC	Cat# CCL-247
EOL-1	ECACC	Cat# EC94042252-F0
SUDHL4	DSMZ	Cat# ACC 495
SUDHL6	DSMZ	Cat# ACC 572
SUDHL8	DSMZ	Cat# ACC 573
WSU-DLCL2	DSMZ	Cat# ACC 575
Toledo	ATCC	Cat# CRL-2631
Pfeiffer	ATCC	Cat# CRL-2632
B95.8 EBV-transformed B lymphoblastoid cell lines (LCLs)	Horie R.	N/A
293T	Watanabe T.	N/A
293FT	Yamochi T.	N/A
Experimental Models: Organisms/Strains		
NOD.Cg-*Prkdc*^{scid}*Il2rg*^{tm1Sug}/*Jic* (NOG) female mice	In-Vivo Science Inc	N/A
Non-obese diabetic (NOD)/severe combined immuno-deficiency (SCID) female mice	Charles River	Strain code 394
Oligonucleotides		
See Table S1	N/A	N/A
Recombinant DNA		
CS-RfA-EVBsd	RIKEN	Cat# RDB06090
pENTR4-H1	RIKEN	Cat# RDB04395
pCAG-HIVgp	RIKEN	Cat# RDB04394
pCMV-VSV-G-RSV-Rev	RIKEN	Cat# RDB04393
pSINsi-U6	TAKARA	Cat# 3661
pGP (gag-pol coding)	TAKARA	Cat# 6161
pE-ampho (env coding)	TAKARA	Cat# 6161
pRx-puro	Watanabe T.	N/A
Software and Algorithms		
FlowJo	FlowJo LLC	9.9.5
R	The R Foundation	3.2.3
DAVID Bioinformatics Resources	https://david.ncifcrf.gov/	6.8
GeneSpring	Agilent Technologies	12.5
GraphPad Prism	GraphPad Software	4.03
Scaffold 4	Proteome Software Inc	4.8.6
Other		
ATL gene expression data (Expression array)	Yamagishi et al., 2012	GEO: GSE33615
ATL gene expression data (Expression array)	Kobayashi et al., 2014	GEO: GSE55851
H3K27me3 data in ATL (ChIP-on-chip data)	Fujikawa et al., 2016	GEO: GSE71450
PTCL gene expression data (Expression array)	Iqbal et al., 2010	GEO: GSE19069
DLBCL gene expression data (Expression array)	Tagawa et al., 2005	GEO: GSE16920
RNA-seq data of normal cells and tissues	Roadmap Epigenomics project	www.roadmapepigenomics.org/

LEAD CONTACT AND MATERIALS AVAILABILITY

Further information and requests for resources and reagents should be directed to and will be fulfilled by the Lead Contact, Makoto Yamagishi (myamagishi@edu.k.u-tokyo.ac.jp). The shRNA-expressing lentivirus vectors and expression plasmids for EZH1, EZH2, CARD11, and MYD88 were generated for this study. These resources are shared for research and educational purposes under a Materials Transfer Agreement.

EXPERIMENTAL MODEL AND SUBJECT DETAILS

Cell culture

Primary peripheral blood mononuclear cells (PBMC) were isolated by Ficoll separation (Ficoll-Paque, GE Healthcare). Normal $CD4^+$ T cells and $CD19^+$ B cells were prepared from human PBMC by $CD4^+$ T Cell Isolation Kit and B cell Isolation Kit II, respectively (Miltenyi Biotec). The immunopurified cells were confirmed by flow cytometry. Co-stimulation of T cells through the TCR/CD28 was induced by plate-immobilized anti-CD3 (1 μg/ml) and anti-CD28 (5 μg/ml) monoclonal antibodies (Miltenyi Biotec). BCR pathway activation was performed by anti-IgM antibody (+, 2 μg/ml; ++, 10 μg/ml; treatment for 48 h) (Jackson Immunoresearch Laboratories).

Lymphoid cell lines and primary lymphocytes were cultured in RPMI1640 (GIBCO) supplemented with 10% of FBS (GIBCO) and antibiotics (GIBCO). 293T, 293FT, and MCF7 cells were maintained in DMEM (Nissui, Japan) with 10% of FBS and antibiotics. G401, TOV21G, NCI-H226 cells were cultured according to manufacturer's instructions. All cell lines and primary cultures were maintained at 37°C with 5% CO_2.

Clinical samples

PBMC from ATL patients, asymptomatic HTLV-1 carriers, and healthy volunteers were isolated by Ficoll separation and maintained in RPMI1640 supplemented with 10% self-serum or FBS. The PBMCs were a part of those collected with informed consent as a collaborative project of the Joint Study on Predisposing Factors of ATL Development (JSPFAD). The study was approved by research ethics committee of the University of Tokyo. Frozen biopsy tissues from patients with DLBCL were chosen randomly from a collection of specimens obtained during the course of diagnostic procedures. The DLBCL cases were diagnosed according to the WHO classification and subgrouped into the germinal center (GC) B cell or non-GC B cell molecular type based on the Hans immunohistochemistry algorithm (Hans et al., 2004). The DLBCL study was also approved by research ethics committees of the University of Tokyo, National Institute of Infectious Disease, and Tokyo Metropolitan Cancer and Infectious Diseases Center Komagome Hospital.

Chemicals

All EZH inhibitors, including E7438, GSK126, UNC1999, OR-S0, OR-S1, and (*R*)-OR-S2/DS-3201, used in this study were synthesized in house. The selectivity of OR-S1 and (*R*)-OR-S2 was profiled through the panels of 34 histone methyltransferases and 253 human protein kinases (Honma et al., 2017).

METHOD DETAILS

Cell-free assay to detect methyltransferase activities

Methyltransferase activity of PRC2-EZH2 and PRC2-EZH1 *in vitro* was monitored by the incorporation of tritium-labeled methyl group from S-adenosylmethionine (^{3}H-SAM) to biotinylated H3 peptide substrate using Scintillation Proximity Assay (Honma et al., 2017). PRC2-EZH2 was prepared as previously described (Cao and Zhang, 2004) or purchased from BPS Bioscience (San Diego, CA, USA). PRC2-EZH1 was purchased from BPS Bioscience. Twenty-five microliters of reaction mixture (50 mM Tris-HCl, pH 8.8, 5 mM $MgCl_2$, 4 mM DTT, 0.005% BSA, 0.8 μM SAM, 0.2 μM ^{3}H-SAM, 0.76 μM biotinylated H3 peptide, 1% DMSO, and 4 ng/μL PRC2-EZH2 or PRC2-EZH1) was incubated in streptavidin-coated FlashPlate at room temperature. After 2 h incubation, each well was washed twice with 50 μL of wash-buffer (50 mM Tris-HCl pH 7.5, 150 mM NaCl) and CPM counts were measured using TopCount plate reader. For IC_{50} determination, each compound was serially diluted and added to the reaction mixture. Four-fold serial dilution was adopted for a total 8 concentrations starting at 25 μM. Data were graphed and analyzed with GraphPad Prism ver 4.03 using "sigmoidal dose-response (variable slope)" model.

Cell-based assay to detect H3K27me3 reduction

HCT116 colorectal cancer cells (1,500 cells / 90 μl) were seeded in a 96 well plate and cultured overnight at 37°C under a condition of 5% CO_2. Then 10 μL of medium containing 1% DMSO and varying concentrations of compounds (range = 0.051 nM - 1 μM) were added to the wells. Cells were cultured for 3 days at 37°C under a condition of 5% CO_2. The amount of H3K27me3 was detected using AlphaLISA Tri-Methyl-Histone H3 Lysine 27 (H3K27me3) Cellular Detection Kit (Perkin Elmer) according to the manufacturer's instructions. The signal intensity of each well was measured by an EnVision multilabel plate reader (Perkin Elmer).

Liquid chromatography-tandem mass spectrometry (LC-MS/MS)

Functional PRC2 was purified by anti-EZH2 antibody (3147S, Cell Signaling Technology) co-immunoprecipitation from TL-Om1 cells in the presence or absence of 100 nM (*R*)-OR-S2 for 7 days culture. Components of the purified PRC2 was analyzed by nanoLC-MS/MS [UltiMate 3000 (LC); Q Exactive Plus (MS), Thermo-Fisher]. Proteome data were analyzed by Scaffold 4 software (Proteome Software Inc). EZH2-bound components (weighted spectral counts in control IgG $\leq$ 5 and Fisher's exact test p values $\leq$ 0.05) were selected. Two biological replicates were analyzed and provided the representative data.

Flow cytometry

Single-cell suspensions of cell culture or lymphocytes were stained with fluorescent-labeled antibodies. Apoptosis and cell cycle were analyzed by Annexin V/7-AAD or PI staining. The fluorescence and lentivirus-mediated Venus expression were analyzed by flow cytometry using a FACSCalibur (BD Biosciences). The collected data were analyzed by FlowJo software.

Chromatin immunoprecipitation (ChIP) assay

The cells ($1\sim5 \times 10^6$) were cross-linked with 1% formaldehyde for 10 min at 37°C, washed with PBS, and suspended in SDS-lysis buffer (50 mM Tris-HCl, 1% SDS, 10 mM EDTA, pH 8.1). The lysate was treated with MNase and then sonicated. After centrifugation, supernatants were subjected to immunoprecipitation with specific antibodies. The presence of the target gene promoter sequences in both the input DNA and the recovered DNA was detected by quantitative PCR using gene-specific primers and SYBRGreen (Applied Biosystems). Primers for ChIP-PCR are provided in Table S1.

Chromatin accessibility assay

Chromatin remodeling was evaluated by Chromatin Accessibility Assay Kit (ab185901) with manufacturer's protocol. Briefly, chromatin isolated from inhibitor-treated cells (1×10^6) was treated with nuclease mix (Nse). After DNA purification, PCR amplification was conducted by using *SLA* loci ChIP primers (Table S1). Fold enrichment (FE) was calculated by using a ratio of amplification efficiency of the Nse-treated DNA sample over that of the no-Nse control sample ($FE = 2^{(Nse\ CT\ -\ noNse\ CT)} \times 100\%$).

RNA isolation and RT-PCR analysis

Total RNA isolation was performed using TRIzol (Thermo Fisher Scientific) or ISOGEN (Wako). DNaseI-treated total RNA was subjected to reverse-transcriptase (RT) reaction using SuperScript II (Thermo Scientific) with manufacturer's protocol. Random primers-based synthesized cDNA was analyzed by quantitative PCR using real-time PCR system (Thermal cycler Dice, TAKARA). The specific PCR was performed using gene-specific primers (Table S1) and SYBRGreen. The levels of *RPL19* or *ACTB* mRNA were also quantified for internal control. Quantification of mature miR-31 was performed by MicroRNA Assays (Applied Biosystems) with manufacturer's protocol. *RNU48* was tested as a control small RNA.

Vectors

Replication-defective, self-inactivating lentivirus vectors (CS-H1-Venus-IRES-Bsd) were provided from RIKEN, BRC, Japan. shRNA-encoding oligonucleotides (Table S1) were cloned into a CS-RfA-EVBsd vector via pENTR4-H1. The established viral vectors were co-transfected with the packaging plasmid (pCAG-HIVgp) and the VSV-G- and Rev-expressing plasmid (pCMV-VSV-G-RSV-Rev) into 293FT cells. High-titer viral solutions were prepared by centrifugation-based concentration and used for transduction into cell lines or primary cultures. The infection was attained by spinoculation method (1,800 rpm, 2 h) and then cultured in appropriate condition for 5 to 7 days. After cultivation, Venus expression of complete cultures was confirmed. For selection of the transduced population, 10 μg/ml of Blasticidin was used. Retroviral vectors (pSINsi-U6, TAKARA) were established by insertion of synthesized oligonucleotide using BamHI and ClaI sites. Retrovirus production was carried out in 293FT cells with pSINsi-U6 (TAKARA), pGP (gag-pol coding), and pE-ampho (env coding). At 48 h post-transfection, retrovirus solution was 0.45 μm filtrated and immediately used to target cells. Transduced cells were selected with 0.5 mg/ml of G418 for 7 days. Only previously validated shRNA sequences (from original articles, siRNA databases, or company websites) were employed in this study. The knockdown efficiency was confirmed by immunoblotting and qRT-PCR.

Transient transfection of EZH1 and FLAG-tagged EZH2 cDNA was performed by Lipofectamine 2000 (Thermo Fisher Scientific). *EZH2* promoter sequence was amplified from human genomic DNA region, checked the sequence, and sub-cloned into pGL4.10 (Promega) (Fujikawa et al., 2016). For stable expression of *EZH2*, *CARD11* or *MYD88*, the N-terminal FLAG-tagged cDNA was inserted into pRx-puro vector. Point-mutagenesis for mimicking the gain-of-function mutations was accomplished with PrimeSTAR Mutagenesis Basal Kit (TAKARA) and specific primer sets (Table S1).

NF-κB analysis

NF-κB target gene set (RelA and RelB) was determined by data integration with (1) expression changes by NF-κB inhibitor DHMEQ, and (2) ChIP-chip peaks with RelA and RelB antibodies. Cellular NF-κB activity was evaluated by lentivirus-based NF-κB-luciferase reporter systems. The luciferase activities were quantified by the Dual-Luciferase Reporter Assay System (Promega).

Immunoblotting and immunoprecipitation

Cellular proteins were analyzed by immunoblotting. For collection of PRC2, SUZ12 immunoprecipitation was performed. Nuclear fraction was prepared by sequential lysing with hypotonic buffer (10 mM HEPES-KOH, pH 7.9, 1.5 mM $MgCl_2$, 10 mM KCl, 0.5 mM DTT, Protease inhibitor cocktail) and hypertonic buffer (20 mM HEPES-KOH, pH 7.9, 1.5 mM $MgCl_2$, 420 mM NaCl, 0.2 mM EDTA, 0.5 mM DTT, Protease inhibitor cocktail). Equal volume of cell lysates was incubated at 4°C for 2 h with 5 μg of anti-SUZ12 antibody (3737S, Cell Signaling) or anti-rabbit control IgG antibodies, followed by incubation with 30 μL of protein G Sepharose beads at 4°C for 1 h. The immunocomplexes were washed four times with the ice-cold lysis buffer and then subjected in

immunoblotting. Immunoblots were performed with primary antibodies. Alkaline phosphatase-conjugated anti-mouse and anti-rabbit secondary antibodies and BCIP/NBT substrate (Promega) were used for detection.

Quantification of HTLV-1 proviral load

Measurement of HTLV-1 proviral load (PVL) of PBMC samples was described previously (Yamagishi et al., 2012). Briefly, quantitative multiplex real-time PCR was performed with two sets of primers specific for the HTLV-1 provirus and the human gene encoding the RNase P enzyme. The PVL was expressed as copy numbers per 100 PBMCs, based on the assumption that infected cells harbored one copy of the integrated HTLV-1 provirus per cell.

Cell growth assay

For evaluation of anti-growth activity of EZH inhibitors, lymphoma cell models (2×10^5), solid tumor models (1×10^4), and LCLs (2×10^5) were plated in 12 well flat bottom plate with optimized medium with 10% of FBS and simultaneously treated with indicated does of compound solution in DMSO for 14 days. The cells were maintained by passage into fresh medium every 3 to 4 days. Primary PBMCs from ATL patients (2×10^5 cells/ 300μl of RPMI1640 with 10% self-serum and 10 ng/ml IL-2) were treated with indicated dose of inhibitors for 7 days. The cell numbers were evaluated by Cell Counting Kit-8 (Dojindo, Japan) following the manufacturer's protocol. Drug efficacy against HTLV-1 infected population was evaluated by changes of provirus load and phenotypic analysis after 10-12 days treatment.

In vivo xenograft studies

Non-obese diabetic (NOD)/severe combined immuno-deficiency (SCID) female mice, 4 weeks of age, were obtained from Charles River Japan (Tokyo, Japan) and NOD.Cg-*Prkdc*^{scid}*Il2rg*^{tm1Sug}/*Jic* (NOG) female mice, 5 weeks of age, were obtained from In-Vivo Science Inc. (Kawasaki, Japan). The mice were housed in autoclaved polycarbonate cages with paper chip bedding covered with filter caps within isolation cabinets and fed a sterile, irradiated diet with free access to acidified autoclaved water (pH 2.5–3.0). Animal room was maintained under barrier-sustained conditions and controlled temperature ($23 \pm 2^\circ$C) and lighting (12-h light/dark cycle). After 1 week preliminary care, mice were used for experiments. This study was carried out in strict accordance with the Guidelines for Proper Conduct of Animal Experiments, Science Council of Japan (http://www.scj.go.jp/en/animal/index.html). All animal procedures and their care were approved by the Animal Care and Use Committee of Rakuno-Gakuen University in accordance with the Guide for the Care and Use of Laboratory Animals.

TL-Om1 cells (1×10^8 per mouse) were inoculated subcutaneously in the post-auricular region of NOD/SCID mice (5 weeks of age). OR-S1 was suspended in the 0.5 (w/v) % methylcellulose solution and administered orally (200 mg/kg, daily). The tumor volume was calculated as 1/2 × (tumor length) × (tumor width)^2. For evaluation of anti-tumor growth activity, TL-Om1 cells (1×10^8 per mouse) were inoculated subcutaneously in NOG mice (6 weeks of age). After the confirmation of tumor establishment (at day 14), the tumor-bearing mice were divided by stratified randomization into each group and dosing initiated. OR-S1 was administered orally (100-200mg/kg, daily) and the tumor volume was calculated daily. After euthanasia, tumor metastasis was also evaluated.

ChIP-chip experiments

All procedures were performed according to the Agilent ChIP-on-chip protocol (v11.0) with slight modification. To ensure the accuracy and biological/clinical significance of the analysis and extract disease-associated epigenetic variations, primary ATL cells with a proviral load of > 100% and > 94% pure resting CD4$^+$ T cells isolated from healthy volunteers were used. The 1×10^7 of primary cells and cell lines were cross-linked in fixing solution. After the washes, cell pellets were resuspended in lysis buffers and then the nuclei were incubated with MNase in 37°C and sonicated for 10 min. The sheared chromatin was incubated with Dynabeads anti-rabbit IgG or Dynabeads Protein G (Thermo Fisher Scientific) coated with either 10 μg of ChIP-grade antibodies (validated by supplier; we also tested by ChIP-PCR assay and immunoblotting) or control IgG for overnight at 4°C. Anti-EZH1 and EZH2 antibodies were previously used and validated for ChIP-seq (Xu et al., 2015b). The antibody-protein complexes were collected, washed and eluted by SDS-containing buffer. The samples were incubated for overnight at 65°C to reverse cross-links and then treated with RNaseA and Proteinase K. The purified DNA was treated with T4 DNA polymerase and then ligated with linker. Two-step linker-mediated PCR was performed and each amplified DNA was used to fluorescent labeling. The labeled ChIP sample and the input chromatin were hybridized to SurePrint G3 Human Promoter Microarrays (Agilent Technologies). After hybridization and scanning, first data mining was performed on the GeneSpring 12.5 (Agilent Technologies). We further selected data entities based on their signal intensity values to remove very low signal values, and then performed normalization (50th or 75th centering based on data distribution) within a batch, allowing comparison among arrays (recommended by Agilent technologies). We further normalized by removing the any variations based on standard deviation. The normalized probes showed positive correlations among same group samples. The mean ChIP signals of each promoter were calculated for several gene set enrichment analyses.

Gene expression analysis

DNase I-treated total RNAs were prepared by TRIzol. Whole gene expression data were obtained by gene expression array (Agilent Technologies). Briefly, Cy3-labeled synthesized cRNA samples were hybridized on 4 × 44K Whole Human Genome Oligo Microarray (Agilent Technologies). The signals were detected by the microarray scanner and analyzed by GeneSpring 12.5. Prior to comparative

analyses in gene expression profiles among tested samples, we conducted appropriate normalization on the set of raw data, i.e., (1) data transformation: set measurement less than 0.01 to 0.01; (2) per chip: normalized to 50th percentile; and (3) per gene: normalize to mean.

DNA methylation analysis

DNA methylation profiles were analyzed using the Infinium MethylationEPIC BeadChip (Illumina) according to the manufacturer's instructions. Methylation data for peripheral blood CD4$^+$ T cells from three healthy controls were used as normal controls. β-values (0∼1) of promoter mCpG (±5kb from TSS) were corrected for probe design bias using a beta-mixture quantile normalization method.

GEO gene expression data

Gene expression profiling of ATL patients, HTLV-1 carriers, and normal CD4$^+$ T cells has been performed previously. The coordinates have been deposited in the Gene Expression Omnibus (GEO) database (GSE33615, GSE55851) (Yamagishi et al., 2012; Kobayashi et al., 2014). For ATL analysis, we have selected diagnosed 49 samples with high PVL (median 78.5% (36.4%–345.8%)). As the control group, freshly isolated CD4$^+$ T cells were obtained from 21 healthy donors, of which ages ranged from 50 to 70 years old. H3K27me3 data from ATL and normal T cells have been deposited (GSE71450, primary ATL cells with high PVL (> 100%) and resting CD4$^+$ T cells isolated from healthy volunteers) (Fujikawa et al., 2016). Gene expression data of PTCL (GSE19069) (Iqbal et al., 2010) and DLBCL (GSE16920) (Tagawa et al., 2005) were obtained from Array Express (https://www.ebi.ac.uk/arrayexpress/). The processed RNA-seq data of normal cells and tissues were obtained from Roadmap Epigenomics project (www.roadmapepigenomics.org/).

QUANTIFICATION AND STATISTICAL ANALYSIS

Significant differences in gene expression, histone methylation, and other biological assays between the two groups were analyzed by Student's t test. Correlations between two groups were analyzed by *Pearson*'s correlation coefficients and probabilities of overlap between gene sets were statistically tested. Statistical significances between two-sample cumulative distributions were calculated by two-tailed Kolmogorov-Smirnov test. Boxplots, beeswarm plots, PCA, and correlation matrix were analyzed and visualized by using R version 3.2.3. Clustering was performed using R package gplots (distance, Pearson correlation; linkage rule, Ward's method). Gene Ontology analysis was performed by DAVID Bioinformatics Resources (https://david.ncifcrf.gov/).

DATA AND CODE AVAILABILITY

The gene expression data and the epigenetic data generated during this study are deposited in GEO with accession numbers GSE138282 (gene expression microarray) and GSE138342 (ChIP-on-chip platform).